



**Politecnico  
di Torino**

# **Politecnico di Torino**

Corso di Laurea Magistrale in Ingegneria Aerospaziale  
A.a. 2021/2022  
Sessione di Laurea Luglio 2022

**Design, Implementation and Optimization of a LQRI  
control for a floating offshore wind turbine in MOST**

**Supervisor:**  
Giovanni Bracco

**Candidate:**  
Christian Di Sannio

**Advisor:**  
Massimo Sirigu

# Abstract

In the last seventy years global demand for energy has led to several problems, most notably air pollution, climate change and natural resources depletion, due to the intense dependence on fossil fuels. Consequently, a large amount of renewable energy technologies are being developed in order to replace fossil fuels and to contrast their huge negative effects. Among them, wind energy appears to be a promising and consolidated renewable alternative. Accordingly, in the last years, many simulators for floating off shore wind turbine (FOWT) have been developed. For the aim of this work, a controller for the simulator named MOST, developed by MOREnergy Lab, has been designed. One of the controller equipped to MOST is a baseline PI controller, developed by NREL, which is a simple use controller. However, for this thesis' project, its low capacity to stabilize the power production around its nominal value has been identified as a limit to overcome. Moving from such limitation, the research focus is to develop a likewise simple use controller to solve such an issue. The new controller is an LQRI developed on a State Space linear representation of a FOWT.

The methodology of research started by the analysis of LQR in order to understand its function. Then after, the analysis proceeded with a simplification of the mathematical model which describes the physics and the mechanism of FOWTs. From such a simplified model, the LQR controller has been first developed, and then optimized through an integral action which has generated a new controller named LQRI.

This new controller, resulted in both the stabilization of the power production, which was a limitation of the controller, and further, through the addition of different modules it has been showed its capacity to work in different operative conditions.

The first chapter will introduce some basic aspects of wind turbines and it will trace back the evolution of the energy market. Additionally, an estimation of the scenario in the next years will be provided to investigate the future development of such a technology.

The second chapter will focus on state-of-art FOWTs mathematical models taking into account their aim, pros and cons. Furthermore, it will introduce some state-of-art mathematical controllers like PI and NREL/ROSCO, clarifying the choice to develop a LQR controller in this work.

The third chapter will introduce some basic information about MOST. It will proceed showing the rationale of the linear representation outlined and the design process of

the LQR controller. Additionally it will illustrate the results through a comparison of the two controllers applied to MOST.

In the fourth chapter different optimizations of the model will be explored and presented. Firstly, the LQRI controller will be investigated and implemented. Secondly, results about linearization with different wind speeds and a gain scheduling controller will be analysed. The results of the addition of the control torque input will be as well discussed.

In conclusion, the last chapter will compare the results of the baseline PI controller and the new controller developed. An explanation about the simplifications of the model will be provided to show how, deleting them, a more accurate controller may be realized.

# Table of Contents

## Chapter I

### Introduction to off-shore wind energy

1.1	Wind energy overview _____	1
1.2	Global wind energy trend _____	2
1.3	Actual and future trend of offshore wind energy _____	3
1.4	Renewable energies variability _____	5
1.5	Floating platforms _____	7

## Chapter II

### Off-shore wind turbine mathematical models and controllers

2.1	Computational methods _____	10
2.2	Structural dynamics _____	11
2.3	Hydrodynamics _____	12
2.4	Aerodynamics _____	12
2.5	Typical software for FOWT _____	13
2.6	Common FOWT controllers _____	15
2.7	Linear controller _____	17

2.8	State-Space representation	18
2.9	Linear Quadratic Regulator LQR	20

## Chapter III

### Linear model development

3.1	MOST	22
3.2	MOST results	24
3.3	State-Space linear model	27
3.4	Linearized coefficients	29
3.5	State-Space model for floating offshore wind turbines	31
3.6	State-Space model simulation	33
3.7	LQR for floating offshore wind turbines	35
3.8	Implementation of LQR in MOST	38

## Chapter IV

### LQR controller and linear model optimizations

4.1	LQR with Integral action LQRI design	43
4.2	LQRI gain matrix calculation and optimization	46
4.3	LQRI results	47
4.4	Pitch stabilization with LQRI	50
4.5	Control torque design for LQRI	52
4.6	Gain scheduling for LQRI	53

4.7	Control switch	58
4.8	LQRI with control switch without gain scheduling	62

## Chapter V

### Analysis' assumptions

5.1	General analysis' assumptions	65
5.2	State-Space model with non-constant water radiation dumping coefficients	67

Conclusions	70
-------------	----

Bibliography	72
--------------	----

# Chapter I

## Introduction to off-shore wind energy

In the last seventy years global demand for energy has led to several problems, most notably air pollution, climate change and natural resources depletion due to the intense dependence on fossil fuels. Consequently, a large amount of renewable energy technologies are being developed in order to replace fossil fuels and to contrast their huge negative effects. Among them, wind energy appears to be a promising and consolidated renewable alternative. This energy technology is effectively becoming a reliable solution among renewable energies. The first chapter will introduce some basic aspects of wind turbines such as their functioning and the pros and cons of their application. It will trace back the evolution of the energy market, with particular regard to Europe, in the last decade to estimate the share of consumption that wind energy can provide nowadays. Additionally, an estimation of the scenario in the next years will be provided to investigate the future development of such a technology.

This work focus on floating offshore wind turbines (FOWTs), and will be followed by a brief explanation of what are their most common offshore configurations, geometrical and performance parameters [1].

### 1.1 Wind Energy Overview

Wind turbines are devices which convert kinetic energy deriving from wind into electricity. Their functioning starts by the rotation of carbon-fibre blades hit by the wind. This rotational energy is then transferred to a gearbox that transform this slow speed rotational energy into higher-speed rotatory motion. This motion is after transferred to a drive shaft which powers the electricity generator. Then, the electrical energy is collected through underground cables and delivered to energy distribution centres. Wind turbine can be onshore or offshore and both configurations are

characterized by pros and cons. Onshore wind turbine are relatively cheap, easy and quick to install and to repair in comparison to the other wind turbine type. Moreover, the short distance between the windmill and the energy distribution centres allows a lower voltage drop off on the cabling, compared to the off-shore wind turbines. Conversely, offshore wind turbines can collect more energy than their counterparts. This positive effect derives from the fact that FOWTs often tend to be installed far away from the coast. That allows the creation of bigger wind farms due to the possibility to build larger and taller wind turbines. In addition, in the outer sea, the wind speed is greater than on land and the wind farm installation tend to be less intrusive for landscapes and human activities around. Furthermore, wind turbines are never built in shipping lanes or fishing areas. Contrarily, onshore wind turbines are often installed near farmlands and can be pretty visible from residential areas. This can have a negative impact on noise and visual pollution for nearby communities but also on farm's ecosystems [2]. In this work, the development of a control system for an offshore wind turbine simulator will be the basis to frame on offshore wind energy as sustainable energetic solution for the future.

## **1.2 Global wind energy trend**

In the last decades  $CO_2$  emissions have reached critical levels. In fact, it has been estimated that last non-renewable energy sources will be drained in the next two or three decades. To face this problem, several eco-friendly and renewable energy production methods have been recently developed. Wind energy embodies a powerful solution among many renewable energy options. Indeed, in the last twelve years, wind energy industry experienced a huge growth. As a matter of fact, global cumulative wind power capacity increased from 159 GW (in 2009) [3] to 837 GW (in 2021). In 2021 the wind industry added almost 94 GW of global cumulative wind power capacity, benefiting of its second best year ever, despite the COVID-19 pandemic [4]. Europe is among the world's largest wind market, after China and USA. Indeed, European countries installed in total 17 GW of new wind energy capacity in the last year. UK is the country that invests the most in wind energy. In fact, the EU-27 (the 27 European Union countries after the UK left the EU) installed 11 GW, whereas UK installed the 28% of the total new European wind energy capacity. The figure below shows the evolution of wind energy capacity in Europe in the last eleven years. Further, the bar chart underlines how onshore installations are still the majority, however, the percentage of installation of new offshore wind turbines is increasing year by year.

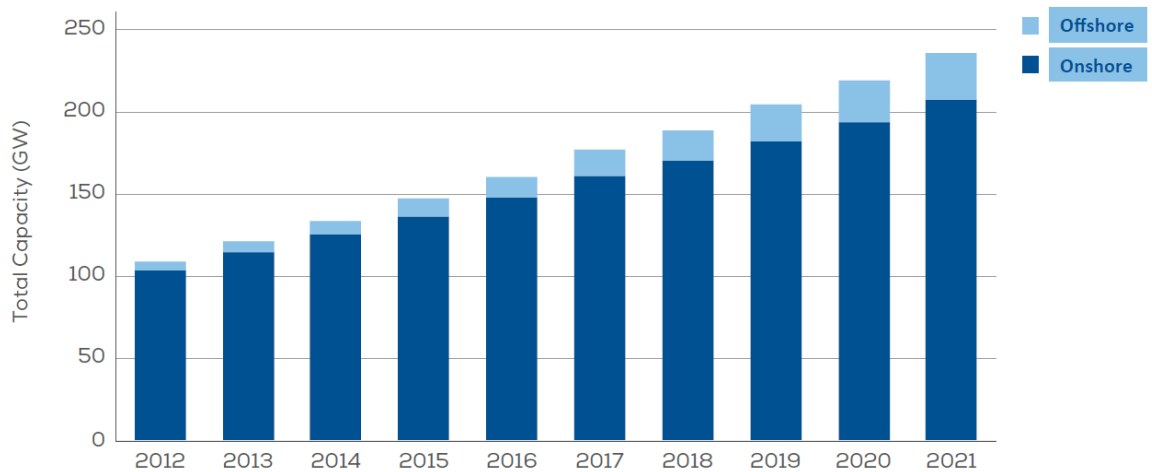


Fig. 1 The growth of total wind energy capacity in Europe 2012-2021 [5]

Unfortunately, this is even not half of what the EU should build to be on track to deliver its 2030 Climate and Energy goals [5]. As can be seen in the table below, using wind energy, Europe is able to meet only the 15% of its electricity consumption.

Europe electricity consumption [TWh]	2921
Onshore wind energy production [TWh]	357
Offshore wind energy production [TWh]	80
Total wind energy production [TWh]	437
Share of consumption met by wind energy [%]	15

Tab.1 Electricity production from wind power in the EU+UK [5]

### 1.3 Actual and future trend of offshore wind energy

From the analysis of last year' data about global wind energy capacity clearly emerges that, in 2021, offshore wind power capacity was 57 GW which represents the 7% of global installations [4]. In 2021, Europe installed 17.4 GW of new wind power capacity; 3.4 GW of these derives from offshore wind installations. This brought total offshore wind power installed in Europe to 28 GW. The experts of the European Wind Energy Association (EWEA) forecasted, in 2021, that almost 10 GW more of offshore wind power capacity will be installed in the next five years in Europe [5] as shown in Fig.2.

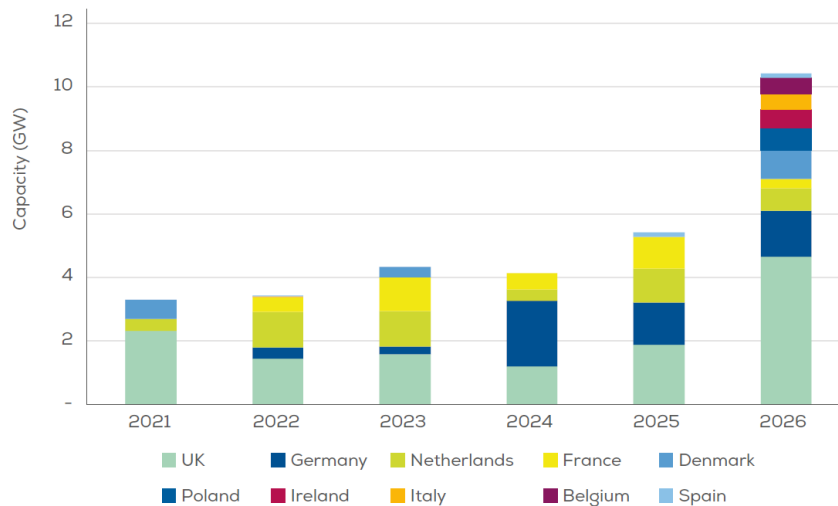


Fig. 2 New offshore installations per country, 2022-26 - Realistic Expectations Scenario [5]

From the analysis of the bar chart of Fig.2 there is a clear evidence that the majority of offshore installations will be built in UK waters. Also Germany, France and Netherlands will strongly contribute to the installation of new offshore wind farms in the next years.

According to the “Offshore Wind Outlook 2019” [6] the best offshore wind sites could supply an amount of electricity that exceed the worldwide total amount consumed nowadays. It has been estimated that the potential of offshore wind is 36,000 TWh per year compared to a current annual global demand of 23,000 TWh, taking into account installations in waters with a bathymetry below 60 m and within 60 km of the coast. Nonetheless, this kind of estimation does not consider external factors such as the transfer of electricity to the ground or issues related to market policies [7]. Conversely, Feng Zhao theorized in “Global Wind Report 2022” [4] that: “ The annual global offshore market is expected to grow from 21.1 GW in 2021 to 31.4 GW in 2026 under current policies, bringing its share of global new installations from today’s 22.5% to 24.4% by 2026. Despite two years of enormous numbers, the current rate of wind growth is simply not rapid enough to allow the world to reach its Paris Agreement targets or a net zero by 2050 goal. Given the energy system reform packages underway in Europe and other regions, in light of the Ukraine crisis as of Q2 2022, GWEC Market Intelligence notes that its five-year forecast could be significantly revised upward this year.”. Drawing from such premise it is possible to state that offshore has the potential to be one of the best renewable energy resource in the next future. However, a further wind market and technology growth is required in order to efficiently supply the current annual global energy demand.

## 1.4 Renewable energies variability

Wind technology progress, thanks to the use of larger offshore wind turbines, has led to the increase of the capacity factor (an index that describes the average output over the year relative to the maximum rated power capacity). Additionally, the values of capacity factors registered in 2018 show that the electricity production of offshore wind energy is almost equal to gas- and coal-fired power plants technologies [7]. As can be seen in Fig.3, in 2018, offshore wind energy exceeded onshore wind and solar PV in terms of productivity. In fact, as highlighted in "Offshore Wind Outlook 2019" [6], offshore wind energy capacity factor was above 50% in the same year. Whereas the values of onshore and solar photovoltaics (PV) ones respectively were around 45% and 20%.

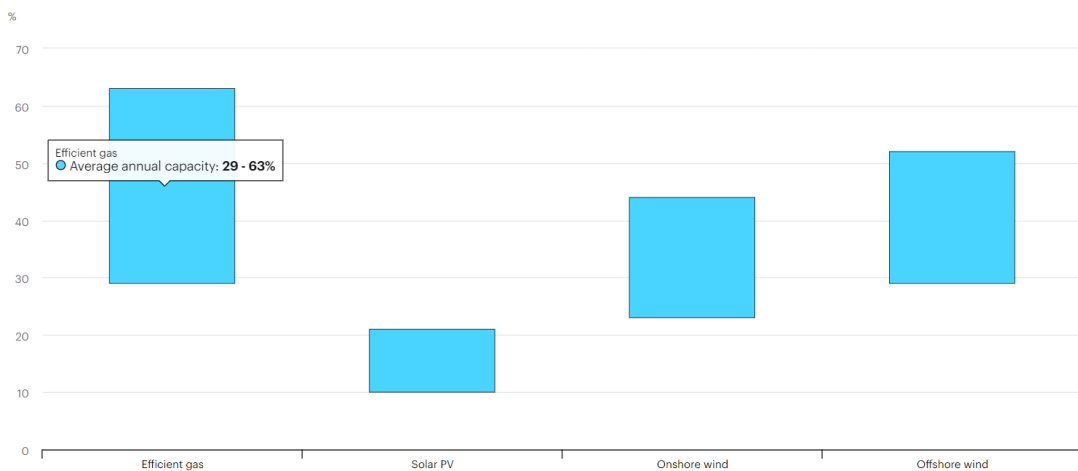


Fig. 3 Average annual capacity factors by technology, 2018 [7]

Nevertheless, it is important to highlight that wind production strongly depends on winds variability. Despite that, it is a matter of fact that its hourly variability is lower than solar photovoltaics. Indeed, wind energy technology has a hour to hour fluctuation of 20% instead of the solar PV fluctuation which is around 40%. Another advantage of offshore wind turbines is their possibility to produce electricity 24 hours per day. Furthermore, the period in which the productivity increases vary according to the geographical area, noteworthy the winter in Europe, US and China and the monsoon in India.

As shown in the figure below, power production is linked to the variability of the wind determining considerable variations from week to week over the course of a year. Moreover, due to the fact that the seasonality of offshore wind is complementary to that of solar PV, such a seasonal compatibility allows the combinations of the two technologies to supply the same area [7].

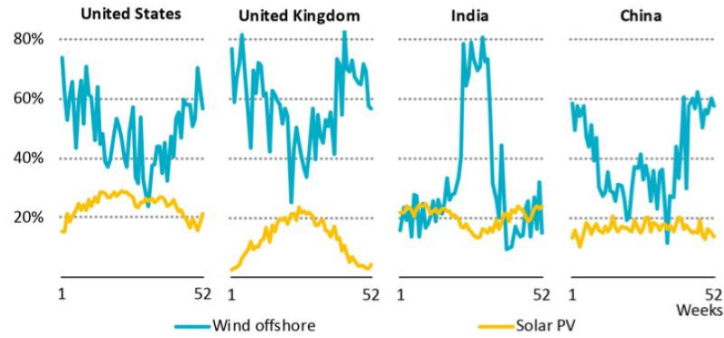


Fig. 4 Simulated average weekly capacity factors for offshore wind and solar PV projects by region [6]

It is also important to point out that the wind resource is strongly affected by geographical wind turbine position, specifically by latitude. Accordingly, near the poles, the wind resources are more efficient than near the equatorial regions. As reported in Fig.5, FOWT average capacity factors values around 45-65% (which is the highest value) in the regions of Europe's northern seas and South America and New Zealand's southern seas, 40-55% in the United States, 35-45% in China and Japan and 30-40% in India [7].

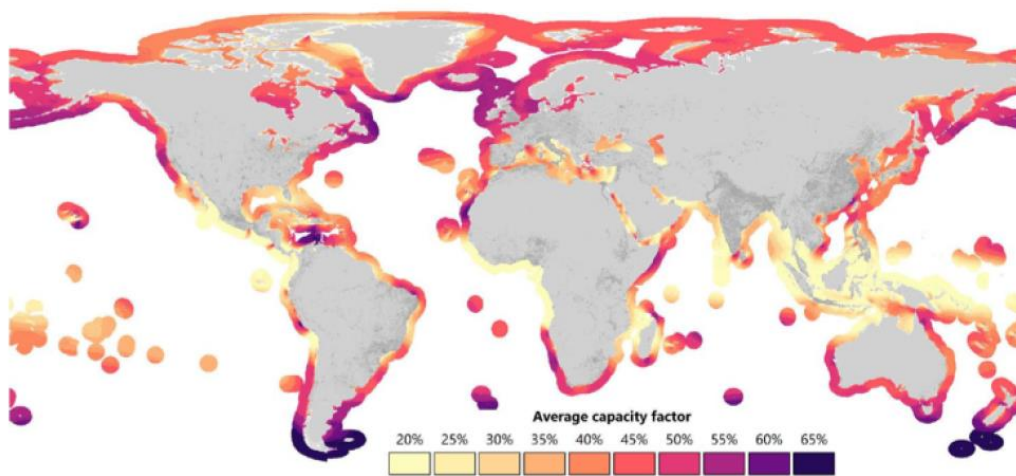


Fig. 5 Average simulated capacity factors for offshore wind worldwide [7]

To date, offshore wind turbines have been installed mostly in shallow waters. These turbines have fixed-bottom foundations because this kind of configuration is quite simple and economic to install in waters with depths of less than 50 m. However, in deeper waters, this kind of choice is not cost-effective. The necessity to install wind turbines in deeper waters derive from the greater wind speed which is registered far away from the coast. As a consequence, the power production increases and the

landscape spoiling is limited. In order to install wind turbines in water that are deeper than 50 m a floating platform is required because this kind of substructure reduces installation costs and guarantees a higher wind turbine stability [1].

### 1.5 Floating platforms

As explained before, offshore wind turbines can be equipped by different kinds of platforms that can be classified in two categories namely fixed bottom foundations and floating platforms. As pointed out in the previous section, thanks to floating platforms, it is possible to generate more power due to the fact that far away from the shore the wind speed is higher. The theoretical debate about different kind of floating platforms has resulted in different concepts, though the most used nowadays are the following:

- Tension-leg platform (TLP)
- Semi-submersible
- Spar buoy

The three kinds of platforms are showed in Fig.6; the barge configuration is discussed in this work.

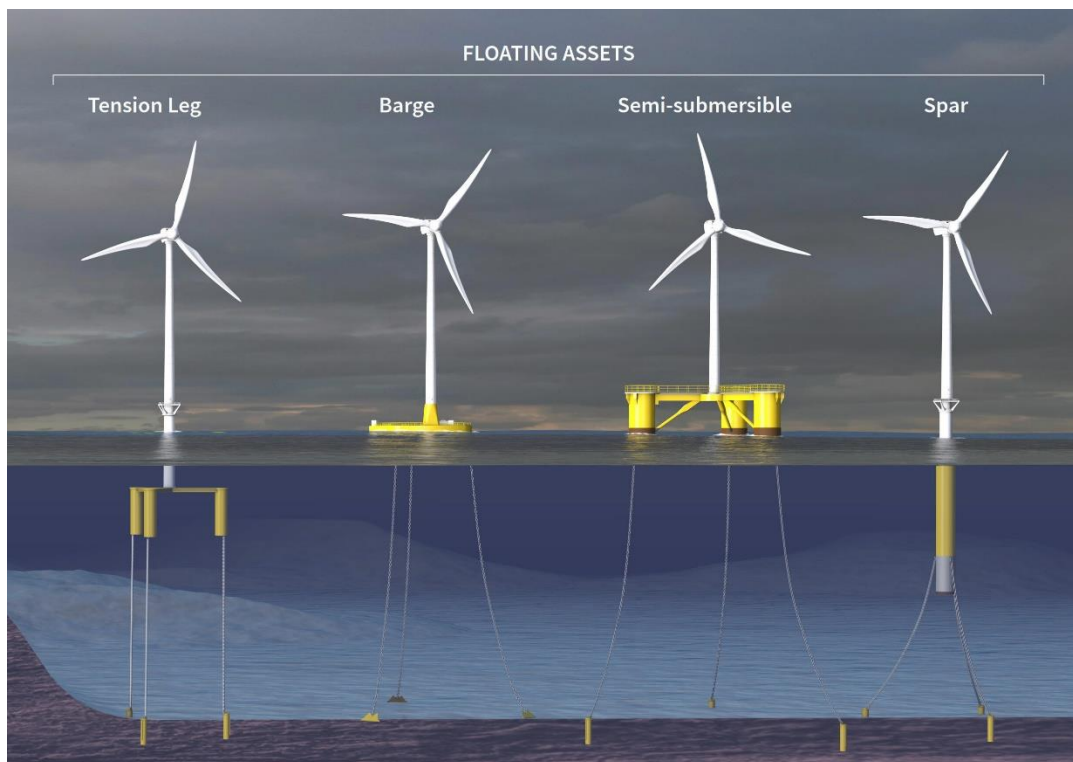


Fig. 6 Most common Floating Offshore platforms [8]

The three different concepts have different characteristics. The spar-buoy is the simplest platform: easy to fabricate, quite stable and with a low mooring cost installation. Even though, a FOWT equipped with a spar-buoy platform results to be heavy and unstable during its transportation in operational area. This aspect makes the turbine difficult to install and to move it back to the shore, in case of major-maintenance issues. In addition, special heavy-lift vessels are required to manage a spar-buoy wind turbine. On the contrary, the TLP is the most stable among all the possible configurations, due to the beneficial effect of the wind which stabilizes its floater pitch motion. Moreover, its taut mooring lines fixed to the sea-bottom contribute to guarantee a high stability and low wave-induced motions. Another plus point is the fact that is quite easy to transport from the shore to offshore operating area. This result in low transportation costs, ease to carry out onshore major-repairs and no need of special vessels for transportation and installation. Nonetheless, the use of this platform has two relevant disadvantages. In one side, the installation cost of this kind of mooring lines and, in the other side, its limitation in operating only in waters deep from 50 m up to 60 m. Comparatively, concerning to semi-submersible platform, a FOWT equipped with this platform is easy to transport and benefits of the same TLP's advantages related to transportation, installation and maintenance. This kind of platform is the less stable compared to the others and it is the more complex to fabricate. However, semi-submersible shape allows to install a wind turbine in shallow or deep waters, guaranteeing to use the wind turbine in a large range of sea-areas [7]. The pros and cons of all these models are summarized in the Tab.2.

To sum up, data shows that in Europe semi-submersible FOWTs are the most common. In fact, floating offshore wind turbine transport and installation costs are prominent aspects and represent the 13% of the complete structure cost. Stating from the fact that, semi-submersible structure installation cost is the lowest, the choice of this offshore floater system implies a significant reduction of the total cost [7]. According to the advantages of such a structure, the FOWTs used in the design of this work' controller is equipped with a semi-submersible platform.

	<b>Tension-leg platform</b>	<b>Semi-submersible</b>	<b>Spar-buoy</b>
<b>Stability</b>	Excellent	Low	Good
<b>Offshore transportation</b>	Relatively easy	Relatively easy	Difficult
<b>Operating water depths</b>	Medium deep waters (50-60 m)	Shallow or deep waters (50 m or more)	Deep waters (100 m or more)
<b>Installation</b>	No special vessel requirements	No special vessel requirements	Requires high-lift vessels
<b>Mooring cost</b>	High	Low	Low
<b>Major-repairs</b>	Relatively easy	Relatively easy	Difficult
<b>Fabrication</b>	Not very complex	Complex	Simple

Tab.2 Advantages and disadvantages of offshore floater systems

# Chapter II

## Off-Shore Wind Turbine mathematical models and controllers

Offshore wind turbines' physical testing is an expensive and challenging task. In fact, the turbine works in two different fluid domains: air and water and, for this reason, one of the most troublesome issue during physical testing is the scaling mismatch between Froude number and Reynolds number. In order to reduce FOWTs design costs, designers developed different mathematical models. This chapter will focus on state-of-art FOWTs mathematical models taking into account their aim, pros and cons. The second part introduces some state-of-art mathematical controllers like PI and NREL/ROSCO supporting the choice to develop a LQR controller in this work.

### 2.1 Computational methods

Modelling floating offshore wind turbines is a challenging task due to the coupling between the structural dynamics of the tower, the aerodynamics of the turbine and the hydrodynamics of the floating platform. It is important to underline that FOWTs are high-priced compared to fixed offshore or onshore wind turbines. For this reason, designers in the drive for cost reduction are using, more and more often, high-fidelity numerical tools reducing both the cost and the time associated with FOWT physical tests. Overall, numerical models are a trade-off between fidelity, accuracy and computational efficiency. Certainly, in the development of a numerical model, an important parameter is computational efficiency which can be described as the amount of time necessary to complete a simulation. Computational efficiency can be also expressed in terms of floating-point operators that describe the complexity of a problem or a dynamical system simulation. However, computational efficiency is

inversely proportional to the fidelity that the method can guarantee. For this reason, numerical methods can be classified into three macro-categories: low-, mid- and high-fidelity. Indeed, it is possible to use a different fidelity method according to the accuracy level required in the stage of the design under examination. Usually low-fidelity tools are used in the first stages because they are simple, fast and cheap. On the contrary, higher level ones are adopted in the last stages or to tune lower level fidelity tools. Furthermore, another possible option is to use a multi-fidelity approach. As anticipated before, simple low-fidelity models are used to simulate linear dynamics of FOWT in the first stages of design and frequency-domain models are the best for this purpose [9]. Certainly, non-linear time domain models can simulate a high-fidelity FOWT response, although this approach is computationally expensive. For this reason, frequency-domain models are commonly used when it is necessary to evaluate different floater designs under several environmental conditions. Nonetheless, they can work exclusively with loads that depend linearly on the response and its derivatives. Common examples of this kind of loads are hydrodynamic added mass loads and hydrostatic loads. Frequency-domain models cannot work directly with non-linear loads like viscous drag or catenary mooring loads. When there is the necessity to introduce these kind of loads, the formulation at the basis of the simulation must be linearized [10].

To sum up, frequency-domain models are useful to calculate hydrodynamic, hydrostatic loads, to perform first stages global simulations and sometimes they can also be used to develop control systems. Conversely, time-domain models are more complex, accurate and computationally expensive, even though they are the best to perform a high-fidelity simulation or to tune a linear low-fidelity model or control system. In the next sections the three most common dynamics modules that constitute a generic FOWT mathematical model will be in depth discussed.

## **2.2 Structural dynamics**

Developing the structural dynamics in a low-fidelity model that tends to capture only rigid-body motions is quite simple. Indeed, simplify the system, as a system made by a composition of only rigid parts, it is sufficient to examine the global system stability. In a more complex model, the elements of the FOWT are typically defined with linear and nonlinear properties. Due to the augmented complexity it is also possible to estimate aerodynamic stability and dynamic response to deformation.

In a high-fidelity time-domain simulations may be necessary to evaluate fatigue and extreme loads in several different extreme/fault/start-up operational conditions. In order to carry out this kind of analysis a FEM (Finite Element Method) is required. Another common approach is to use a modal analysis. In this case some flexible DoFs

(Degrees of Freedom) are represented by their modes and modes shape. For instance, the FAST software uses this method to model the blade and the tower of the FOWT. If it is compelling to understand the interaction between the rigid body and the fluids a BEM (Boundary Element Method) combined with low-order meshing is a suitable choice [9].

### **2.3 Hydrodynamics**

The two most common methods used to model hydrodynamics are: PF (Potential Flow) method and ME (Morison Equation) or a combination of the two. Thanks to these, it is possible to compute first and second-order wave excitations. The calculus can be performed with a reasonable computational efficiency delivering the required accuracy. However, some problems may arise when simulations of complex geometries occur.

Usually, the PF method is adopted to solve radiation and diffraction loads, and further, numerical tools based on PF theory use BEM. Nevertheless, PF methods have some limitations such as viscous effects which are ignored and oscillation amplitudes which need to be assumed as a small value when compared to the ones concerning the cross-sectional area of the floating elements of the body. Generally, time-domain PF solvers require a set of hydrodynamic coefficients imported from a frequency-domain PF solver.

The second method is ME which is typically used for structures composed by slender cylindrical elements. This method can model viscous and inertial loads. Therefore it is possible to simulate elements that are immersed in waves and currents. Unfortunately, Morison Equation has also a limitation because it ignores alteration inducted by the floating body over the incident wave field.

In order to solve more complex problems it is possible to use a combination of PF+ME or high-fidelity CFD (Computational Fluid Dynamics) solvers that are based on Navier-Stokes equations. CFD models are usually applied to solve specific non-linear problems as vortex shedding or slamming loads due to extreme waves and they are computationally expensive [9].

### **2.4 Aerodynamics**

The main challenge of aerodynamic module is to capture the effects of dynamic inflow that can cause an overshoot of rotor thrust loading. These effects can appear due to the motions of the platform causing a variation in relative wind velocity. One of the most efficient methods, used to model aerodynamics effects, it is BEMT (Blade Element Momentum Theory) that combines momentum theory with blade element theory.

BEMT works through the division of the blades of the turbine into smaller strips and, after calculating the aerodynamic proprieties of each element, integrates these values in order to solve aerodynamic proprieties for the entire rotor.

To perform the same calculus, it is possible to use as well high-fidelity PF or CFD methods. The side effect of this choice is the augmented computational cost.

Recently, another widespread method for large blades rotor is the FVW (Free Vortex Wake method). This method can be considered as a cost-effective compromise between BEMT and CFD methos. FVW is also used in the latest version of OpenFAST [9]. A schematic representation of all these modules is summarized in the next figure.

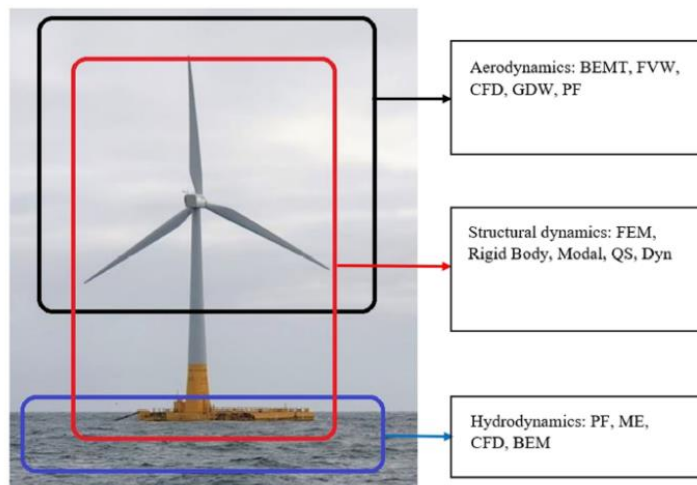


Fig. 7 Schematization of typical approaches for different FOWT modules [9]

## 2.5 Typical software for FOWT

As explained in the previous paragraphs, low-fidelity methods are usually adopted to compute hydrodynamic and hydrostatic loads, to rapidly run a generic simulation or to develop simple and effective controls. Moreover, high-fidelity models (which are only time-domain) can perform more detailed and complex analyses, even though such a model specifically developed for FOWT does not exist. Indeed, to perform such simulations, generic CFD- or FEM-based software can be used. These methods are really difficult to develop and require a lot of time to perform calculus. However, they are suitable to analyse particular/extreme operational conditions or phenomena, to validate a FOWT project in the last stages of the design or to tune lower-fidelity models.

Nonetheless, in FOWTs design are also largely employed other kind of models namely the mid-fidelity ones which are a combination of different methods. These software

can run dynamic analyses both with linear and nonlinear loads. Noteworthy, in this category there is FAST (Fatigue Aerodynamic Structures and Turbulence) that is an open source software developed for research purposes by NREL (National Renewable Energy Laboratory) in the USA. This software “joins aerodynamics models, hydrodynamics models for offshore structures, control and electrical system (servo) dynamics models, and structural (elastic) dynamics models to enable coupled nonlinear aero-hydro-servo-elastic simulation in the time domain” [11]. Moreover, it allows the user to select onshore, offshore fixed-bottom or floating offshore wind turbines. In the last years the software has been improved in its development generating a new and more complex software named OpenFAST. This engineering tool is composed by several modules that can solve the coupled nonlinear aero-hydro-servo-elastic-mooring dynamics of FOWTs in time-domain. Some linearized calculus can be likewise performed with the same tool. Furthermore, both FAST and OpenFAST are codes that use other different engineering tools such as MATLAB, Simulink, Fortran, Python, Git, Visual Studio, etc.

Other similar mid-fidelity software are: HAWC2 developed by the Technical University of Denmark, SIMA developed by Selskapet, Bladed developed by Det Norske Veritas and SIMPACK, a general multi body simulation which interfaces with FAST and Bladed. Most of these mentioned tools require external hydrodynamic coefficients to solve the radiation and diffraction problems. Such coefficients can be provided as input from other frequency-domain solvers such as WAMIT, AQWA or Nemoh [9]. For instance, WAMIT is a software developed by the Massachusetts University of Technology and it is one of the most advanced set of engineering tools able to analyse wave interactions with offshore platforms, vessels or other structures [12]. Another useful tool is WEC-Sim (Wave Energy Converter SIMulator), an open-source software used to simulate wave energy converters which was developed in MATLAB/Simulink using the multi-body dynamic solver Simscape Multibody. WEC-Sim simulates, in time-domain, the response of a system composed by hydrodynamic bodies, a power take-off system, joints, constraints and mooring systems. For higher level simulations, WEC-Sim needs also an external input as hydrodynamic coefficients from WAMIT or similar software [13].

In the last few years, different universities and research centres are working to develop their own FOWT simulator using a combination of many of the above mentioned software. An example is MOST (Matlab for Floating Offshore wind turbine), a fast simulation model developed by MOREnergy Lab for Politecnico di Torino that has been used in this work. In the following table the methods used for the different modules of some of these software can be seen.

Software	Hydrodynamics	Aerodynamics	Structure
FAST	PF + ME	BEMT + GDW/FWW	RB + Modal/FEM + Dyn/QS
HAWC2	PF + ME	BEMT + GDW	FEM + Dyn
SIMA	PF + ME	BEMT	FEM + Dyn
Bladed	With SIMA	BEMT + GDW	Modal
SIMPACK	With HydroDyn	AeroDyn/AeroModule	FEM
Orcaflex	PF + ME	With FAST	RB + FEM + Dyn
Flexcom	PF + ME	With FAST	RB + FEM + Dyn

Fig. 8 Engineering tools used for FOWT modelling [9]

## 2.6 Some common FOWT controllers

Among the several controller for wind turbines, one of the most famous is the Proportional-Integrative (PI) control. This is a control loop mechanism widely used for onshore wind turbines. Generally a PI control is designed with the aim to set the optimal blade pitch angle that guarantees the maximum power production. Many models add a gain scheduling to the PI control, which allows the controller to select the proper gain in relation to the variation of an external parameter. Usually, a gain scheduling in wind turbine controls is developed to optimize the gain according to wind speed changes. A common wind turbine PI control can be expressed in the form of:

$$\theta = K_p \omega + K_I \int \omega dt \quad (1)$$

$\theta$  is the blade pitch,  $K_p$  and  $K_I$  are respectively the proportional and integral gains,  $\omega$  is the turbine rotor speed. Jason M. Jonkman in “Influence of Control on the Pitch Damping of a Floating Wind Turbine” [13] presents different approaches to optimize a PI control for FOWTs, conversely to the common use for onshore wind turbines. In his work, he analysed the design of different versions of a PI control. Taking into account that the PI was born and developed for turbines whose towers have no possibility to move, none of them was able to optimize simultaneously power production and barge-pitch response for the FOWTs. Furthermore, he supposed that a MIMO State-Space controller could be an optimal solution to improve rotor-speed regulation and platform-pitch damping [13].

Nonetheless, blade pitch is not the only parameter through which it is possible to control a FOWT. In fact, the second parameter through which a FOWT can be controlled is the generator torque.

Another famous FOWT controller is the NREL's Reference Open Source Controller (ROSCO) which has a modular architecture with a Python- and Fortran-based structure. Its primary function is to maximize power in below-rated operation and to regulate rotor-speed in above-rated operation. ROSCO controls the power generated through the generator torque and regulates the rotor speed by means of the collective blade pitch angle. ROSCO has also a PI controller which modifies the generator torque, allowing the turbine to maintain a defined minimum rotor speed and avoid blades from exceeding their maximum allowable angular limits. Its gain scheduling improves the power output according to wind speed changes using a windspeed estimator. A schematic example of ROSCO is showed below.

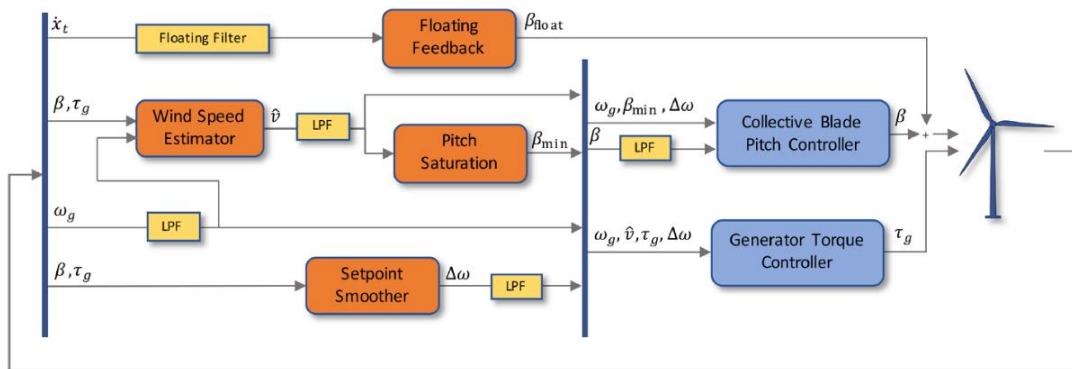


Fig. 9 ROSCO scheme [14]

$\dot{x}_t$  is the tower-top fore-aft velocity,  $\beta$  is the collective blade pitch angle,  $\tau_g$  is the generator torque,  $\omega_g$  is the generator speed,  $\beta_{min}$  is the minimum blade pitch angle,  $\hat{v}$  is the estimated wind speed and  $\Delta\omega$  is a controller reference set point shifting term from the set point smoother. As clearly showed, ROSCO is a multifaced and more efficient controller compared to the PI, indeed it confirms itself as one of the best FOWT controllers [14].

## 2.7 Linear controller

As it was supposed backwards, State-Space based controller could be a good alternative to classical controllers. Indeed, in the article “Two LQRI based Blade Pitch Controls for Wind Turbines” [15] a Linear Quadratic Regulator (LQR) control with Integral action (LQRI) is developed and compared with a common PI control. This LQR has two blade pitch controls: the individual and the collective one and both have different advantages. On one hand, the individual pitch control can reduce the oscillation of the blade bending moment and, on the other hand, the collective pitch can mitigate the magnitude of moments. The conclusion was that the collective pitch controller is efficient for rotor speed regulation and blade load reduction, while the individual one is optimal to decrease load fluctuations on the blades. Moreover, it has been proved that the LQRI controller shows a better performance than a conventional PI-based control. In fact, in the graph it is visible that when a LQRI with the right weighting is used, the overshoot in rotor speed regulation is lower.

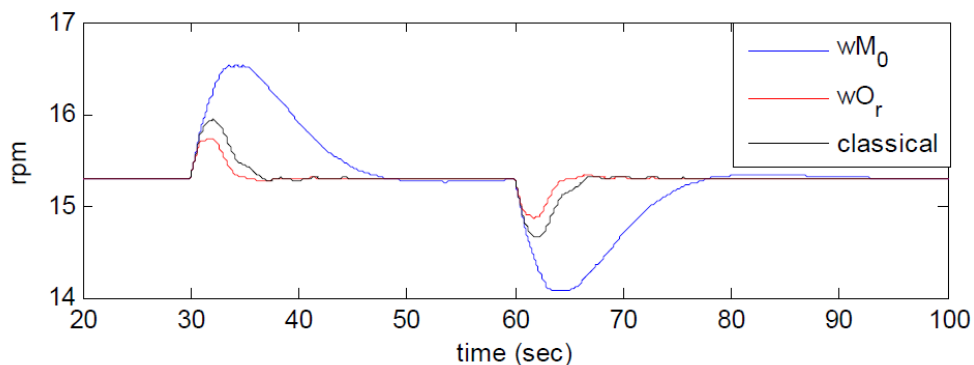


Fig. 10 Responses of rotor speed [15]

In this plot, the black lines indicate a common PI control, the red line a LQRI control developed to reduce rotor speed overshoots and the blue line a LQRI control developed to reduce the momentum magnitude overshoots. Clearly, the LQRI developed to reduce rotor speed fluctuations can be considered as more efficient among the others. The second example is for blades momentum magnitude.

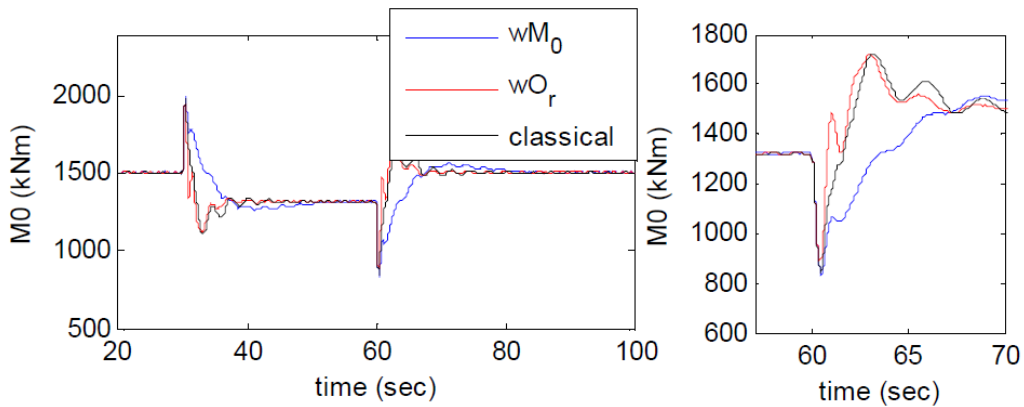


Fig. 11 Responses of collective blade bending moments [15]

As before, it can be noticed that a LQRI control developed to reduce the loads on the blade is the best choice. Though, a trade-off in the LQRI design is required for a complementary optimization of both the rotor speed and the load reduction. According to the article [15], a LQR can be a simple but more efficient alternative to classical wind turbine controls. For this reason, it appears to be the optimal design solution for this work controller. Stating from such a theoretical background, this thesis' work focused on the replacement of a common PI control with a new controller able to overcome its limitations. Indeed, the LQR appeared to be the perfect trade-off between the two controller and it will be in depth described in the following sections.

## 2.8 State-Space representation

The LQR is a type of optimal control based on State-Space representation. State-Space is a method to represent a complex system described by second or higher order differential equations. In this representation, first order equations are repackaged in a set of simple matrices. To write a system in this form, the dynamical system needs to be written in a linear form. The State-Space representation can be expressed both in time- or frequency-domains. The rewriting and repackaging of the high order differential equations into a set of  $n$  first order differential equations is obtained through the writing of all the equations as the first derivative of their following equation. In this way, many variables, named "states", are at most the first derivative of their previous state. This representation can be commonly written as:

$$\dot{x} = Ax + Bu \quad (2)$$

$$y = Cx + Du \quad (3)$$

Where:

Element	Description	Dimensions
$x$	State Vector	$[n \times 1]$
$u$	Input Vector	$[r \times 1]$
$y$	Output Vector	$[m \times 1]$
A	State Matrix	$[n \times n]$
B	Input Matrix	$[n \times r]$
C	Output Matrix	$[m \times n]$
D	Feedthrough Matrix	$[m \times r]$

Tab. 3 Explanation of State-Space representation elements

$n$  is the number of states and represents the number of the new independent variables,  $r$  is the number of inputs and  $m$  is the number of output. It is important to underline that the choice of the states and the inputs is arbitrary. Indeed, the first step to write a State-Space model is to choose which are the variables that will be the states and which ones will be the inputs or the disturbances of the system. This choice has to be made as a function of the effects that are required to be analysed in a physical phenomenon or dynamical system. Hence, the states has to be to the minimum set of variables that can fully describe a system. In other words, the choice of the states is related to the variables that allows to obtain enough information to predict system's future behaviours. The number of outputs is limited arbitrary because it can be at

maximum equal to the number outputs that can be measured by system' sensors [16]. A typical State-Space block diagram representation is showed below.

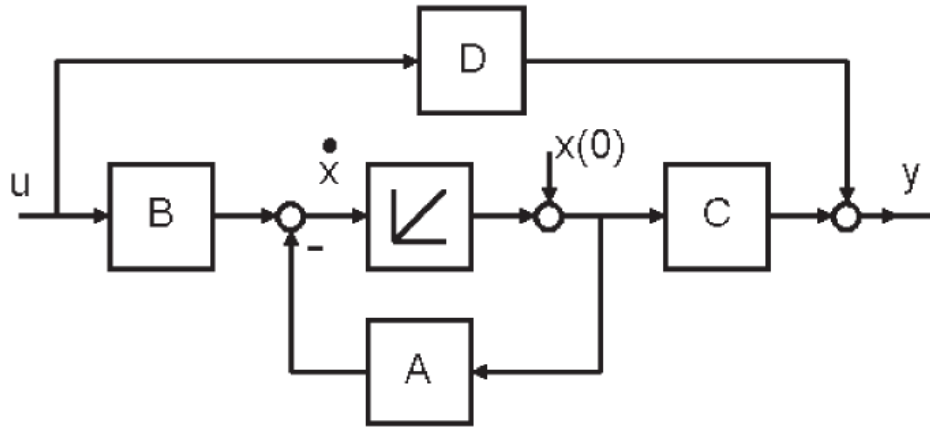


Fig. 12 State-Space block diagram representation [17]

In this representation, the state vector and its derivative change as a linear combination of the states and the inputs. Therefore, once the inputs and the initial conditions are defined, the system computes how the states change during the simulation. Sometimes, a disturbance can also be included in the formulation as described in the following expression:

$$\dot{x} = Ax + Bu + Fd \quad (4)$$

## 2.9 Linear Quadratic Regulator LQR

A State-Space model is not necessarily stable and sometimes could be necessary to control it. To do that, it is possible to use a LQR which is a kind of optimal control that optimizes, in a given time, an objective-function. The purpose of a LQR is to find a gain that, multiplied by the states, generates the new inputs of the system. The inputs are then rescaled as showed in the expression:

$$u = -Kx \quad (5)$$

This gain matrix K is obtained by minimizing the performance index J also called *cost function*. This calculus finds the best trade-off between the system performance and its actuator effort. The cost function is showed in the following expression.

$$J = \int_0^{\infty} (x^T Q x + u^T R u) dt \quad (6)$$

The performance can be thought as the capability to bring a state, in a certain time, from the initial condition to its equilibrium condition. The integral in the formula calculates the area under the curve of the state's evolution over time, which represents how quickly this regulation acts. A smaller area stands for a better performance while a bigger area represents a worse system' performance. The states can have negative or positive values, however, the cost function cannot be negative. As a result of that, states and inputs are squared in the cost function equation which is a quadratic function [18].

It is essential to mention that LQR gain matrix can only be calculated if the system is controllable and observable. Moreover, this LQR can be designed trough the weighting matrices Q and R which are two square and diagonal matrices. Q is the matrix with the weights that penalizes states performance while R is the matrix which penalizes inputs effort. If a Q value is high its state error associated is penalized, that results in a better performance of that state. On the contrary, if a R value is high, the energy resource associated with an input is penalized and this will allow the system to save energy to perform a given action. The following table can give a better understanding of this concept.

Value	Q	R
↑	The states has a better performance	The actuator uses less energy
↓	The states has a worse performance	The input uses more energy

Tab. 4 Schematization of Q and R values characteristics

# Chapter III

## Linear model development

The purpose of this work is to develop a simple and efficient controller for FOWT. The controller was developed to replace the PI controller of the MOST non-linear time domain model. As anticipated before, the new controller is an LQR designed on a State Space linear representation of a FOWT. This linear model is based on linear coefficients obtained from MOST. This chapter will introduce some basic information about MOST. It will proceed as follow: the rationale of the linear representation outlined and the design process of the LQR controller. The last section of the chapter will illustrate the results through a comparison of the two controller applied to MOST.

### 3.1 MOST

“MOST is an innovative non-linear, time domain numerical model for the simulation of offshore floating wind turbines. The model is able to evaluate the movement of the platform in six degrees of freedom, the power production and the load cycles acting on the blades. MOST is implemented in Matlab-Simulink environment using Simscape Multibody.” [19]. As many other simulators for floating off shore wind turbines, MOST is composed by different modules and these are respectively: structure dynamic, aerodynamic, hydrodynamic, mooring and control system modules.

The first module can compute the motion of the platform in 3 or 6 degrees of freedom and calculates the forces acting on the tower, the shaft, the bearings and the blades.

The aerodynamic module uses look-up tables to select the correct aerodynamic forces. The values contained in the tables are calculated according to the blade element momentum theory. The look-up tables illustrate the contribution of each blade to the axial and tangential forces and moments as a function of blade pitch, rotor angular speed and the average windspeed. The values used in the look-up tables come from

FAST simulations, which takes into account a baseline controller assuming that the three variables (wind speed, blade pitch and rotor speed) vary around the steady state point. The following figures show the trend of the forces and moments as a function of the wind speed and rotor speed around the steady state points.

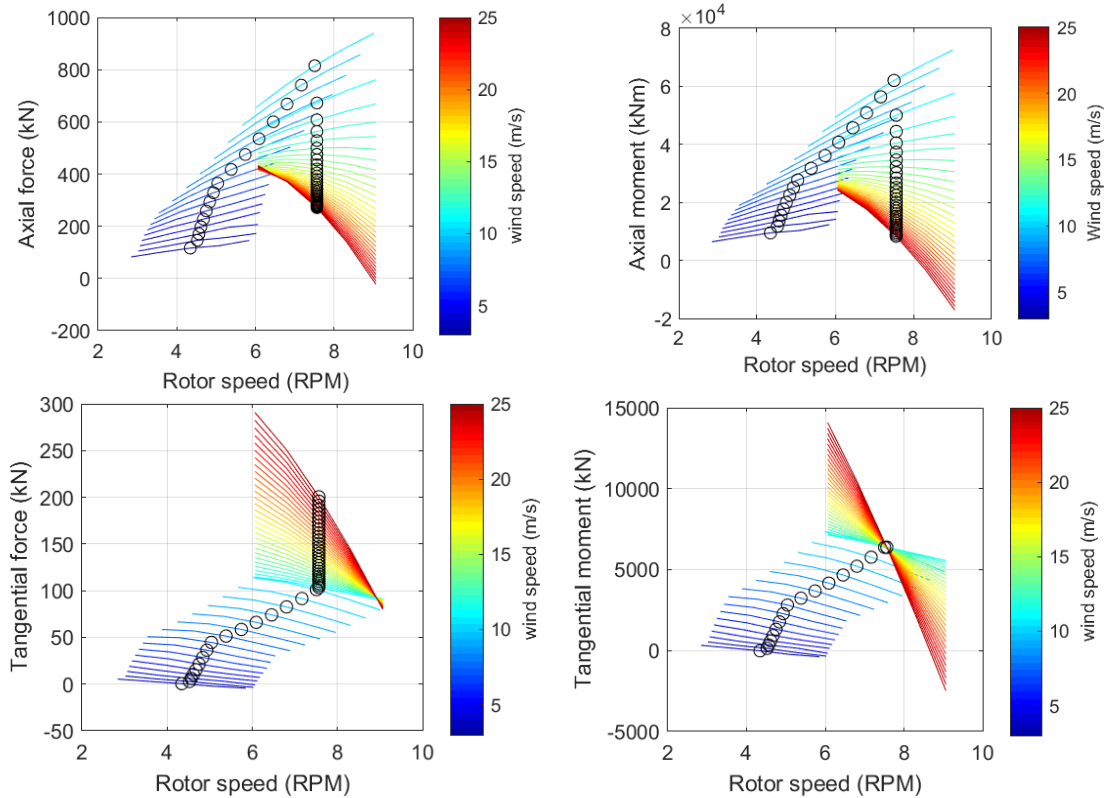


Fig. 13 Example of MOST look-up tables for forces and momentums [19]

The hydrodynamic module uses a Simscape library named WEC-Sim to calculate hydrodynamic forces. WEC-Sim solves the dynamics of the floating bodies through hydrodynamic properties evaluated with external software like Wamit, Ansys Aqwa. The mooring module performs calculi about mooring lines forces.

The control system module includes two different controllers: a baseline PI control and a ROSCO control. Both of them compute the optimal blade pitch and generator torque according to given external and operating conditions. Stating from such a premise, this analysis will focus exclusively on the baseline PI controller according to the aim of this work. The generator torque control law of this baseline controller has been developed with the aim to maximize FOWT power extraction. This control law depends only on the generator speed. Fig. 14 shows the dependence of this function on rotor speed.

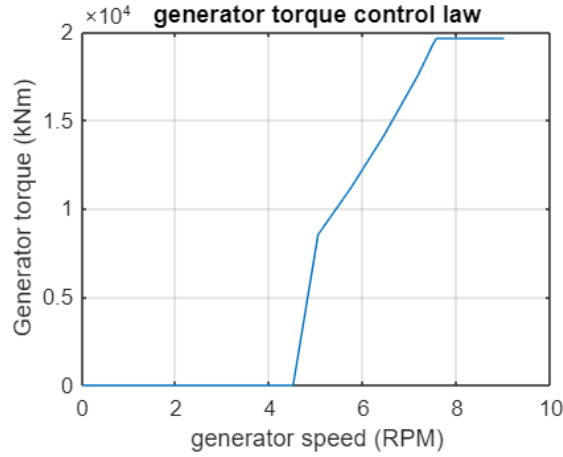


Fig. 14 Generator torque control law [19]

Moreover, the PI blade pitch control uses a gain scheduled for the power regulation. The equation that describes the blade pitch angle control is expressed as following:

$$\theta = K_p \Delta\omega + K_I \frac{\Delta\omega}{s} \quad (7)$$

$$\Delta\omega = \begin{cases} \omega - \omega_0 & \text{if } \omega > \omega_0 \\ 0 & \text{if } \omega \leq \omega_0 \end{cases} \quad (8)$$

Where  $\omega_0$  is the rated generator speed,  $K_p$  and  $K_I$  are the gains for the PI control and are functions of power to pitch sensitivity. This scheduling is crucial because under a certain value wind speed, rotor speed value will be quite low as well. When such occurs, the blade pitch control is not able to grant the generation of the nominal power. In this case there will be only the generator torque control and the PI control will be disabled. This blade pitch controller is the same implemented in FAST [19].

### 3.2 MOST results

In order to design the controller and to develop the linear State Space model, some simplifications have been required. According to the fact that MOST can compute the motion of the platform in 3 or 6 degrees of freedom (DoF), for this work, the platform simulations have been made in 3 degrees of freedom which are Pitch, Surge and Heave. The Yaw, Roll and Sway motions are not considered in this work. The second assumption is that significant waves are neglected. For this reason the parameter  $H_s$ , which represents significant wave altitude, is set to 0 m. The third simplification is that the wind speed is considered as constant. In this simulation the wind speed ( $V_0$ ) has been assumed to be 15 m/s. The selected wind turbine is the Voltorn US 15 MW and

the controller selected for this first simulation is a common PI controller named “baseline NREL controller”.

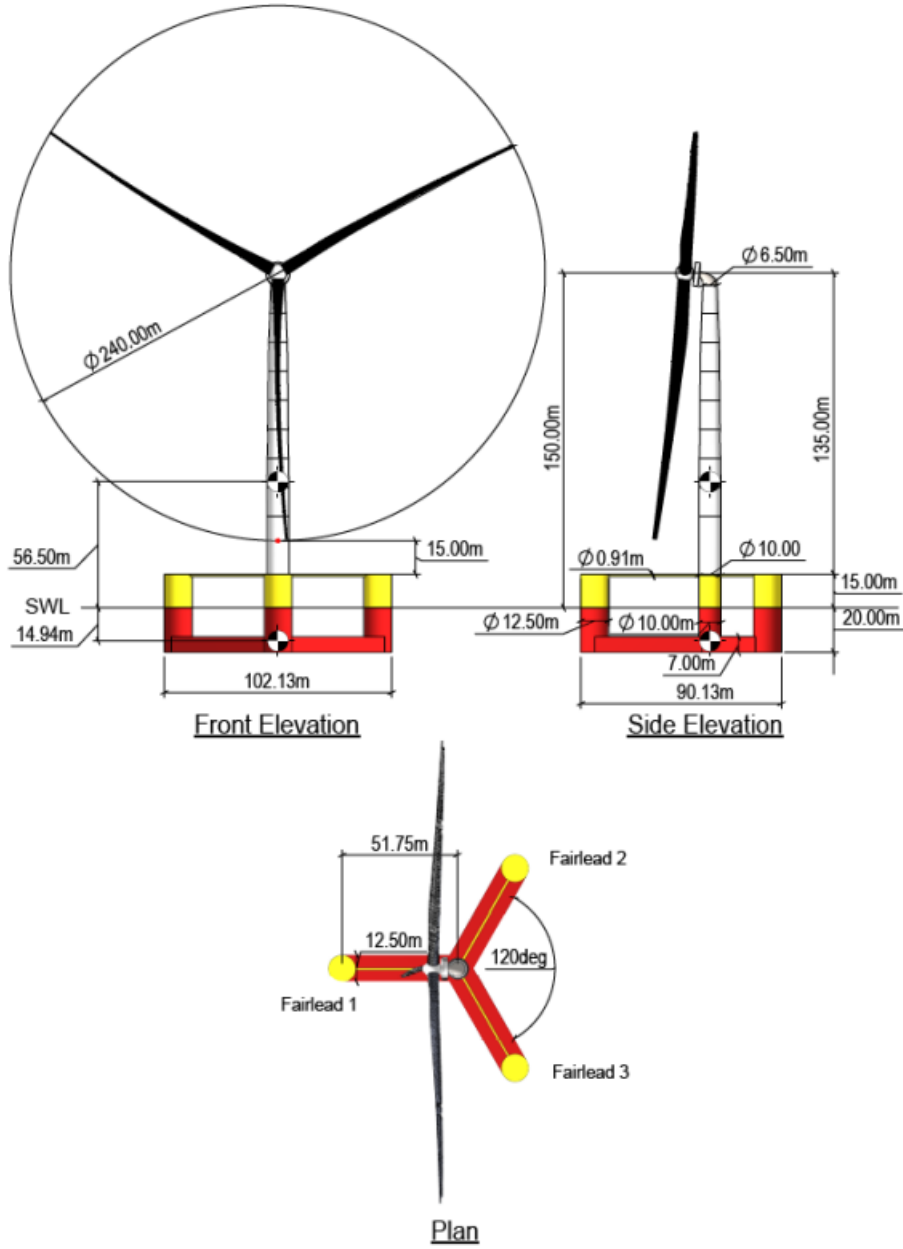


Fig. 15 Voltturn US 15 MW geometrical data [20]

Accordingly, the simulation conditions described above are summarized as follows:

- 3 degrees of freedom floating system
- Significant wave altitude  $H_s = 0 \text{ m}$
- Wind speed  $V_0 = 15 \frac{\text{m}}{\text{s}}$
- Baseline NREL controller (PI)

The results of this simulation are reported in Fig. 16.

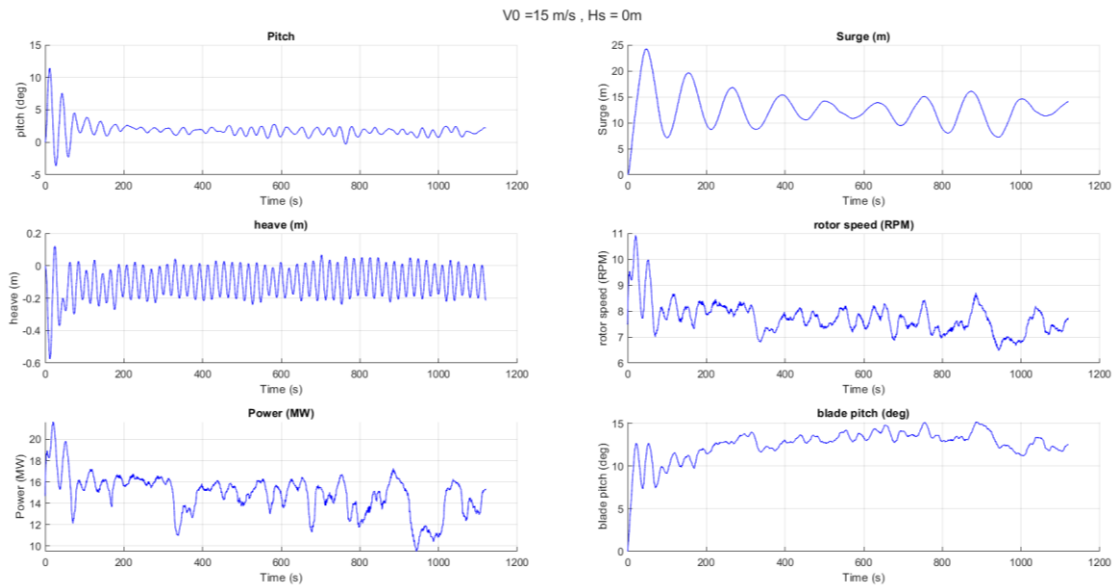


Fig. 16 Results of MOST simulation with baseline NREL controller

As can be seen from the plots reported above, the heave movement has a really small variation if compared to the pitch and the surge. For this reason, this displacement will be neglected in the linear model. Contrarily, pitch and surge movements are not irrelevant but show anyway a stable response. The problem of this controller is that appears to work really well with pitch stabilization but does not work likewise for the power production. Indeed, power fluctuations are quite evident in the graph. The nominal power is 15 MW but the system shows a response with several points in which the power decreases of 3 or 5 MW. Nonetheless, the optimal result would be a power production with smaller fluctuations and a maximum excursion of  $\pm 1 \text{ MW}$  compared to the reference value. The same consideration can be made about the rotor speed whose reference value is approximately 7.55 rpm. In this case an optimal range for the rotor speed would be [7-8] rpm but the response shows that the range in which rotor

speed fluctuates is approximately [6.5-8.5] rpm. Moving from the idea to limit these issues, the purpose of the new controller designed in this work is to reduce as much as possible the power and the rotor speed fluctuations.

### 3.3 State Space Linear Model

The first step to create a simple linearized model is to define the assumptions upon which the system is developed and to write down the equations that describes the physics of the model. The physics of floating off shore wind turbine can be very complex. As stated before, such a model is described by the combination of aerodynamics, structural dynamics and hydrodynamics. In order to simplify this system is required to move from different assumptions. The first two important ones are:

- The platform degrees of freedom considered are two: Pitch and Surge; the other DoFs are considered negligible. This assumption is justified by the fact that, running different simulations in MOST, it appears that these are the only two values which vary significantly.
- The centre of rotation is set at sea water level

The equations that describe how surge and pitch vary are expressed according to a mass-spring-damper model as following.

$$\textit{Surge Equation} \quad M\ddot{S} + c_{rs}\dot{S} + k_{mooring}S = F_{ext} \quad (9)$$

$$\textit{Pitch Equation} \quad I\ddot{\gamma} + c_r\dot{\gamma} + k\gamma = F_{ext}b \quad (10)$$

Given that the surge is a distance, its equation is a force equilibrium equation, while the pitch is an angle and its associated equation is a momentum equilibrium equation. In the second equation, the mass is replaced by the moment of inertia of the wind turbine. An additional equation of momentum equilibrium is needed to express the shaft behaviour.

$$\textit{Rotor Speed Equation} \quad J\dot{\omega} = C_{ext} - C_{gen} \quad (11)$$

$C_{ext}$  is the external torque generated by the wind over the wind turbine blades,  $C_{gen}$  is the wind turbine control torque and  $F_{ext}$  is external force. These forces and torques are expressed as a combination of a constant term plus a linearization of external force and torque according to windspeed, rotor speed and blade pitch. In conclusion, the following expressions can be written as below:

$$F_{ext} = F_0 + c_v(v - \dot{\gamma}b - \dot{s}) + c_\omega\omega + c_t\theta \quad (12)$$

$$C_{ext} = C_0 + k_v(v - \dot{\gamma}b - \dot{s}) + k_\omega\omega + k_t\theta \quad (13)$$

All the terms in the expressions are listed in the table below.

Term	Unit	Meaning
$\gamma$	[rad]	Tower pitch angle
$s$	[m]	Tower surge displacement
$\omega$	[rpm]	Motor rotor speed
$\theta$	[deg]	Blade pitch angle
$v$	[m/s]	Horizontal wind speed
$I$	[kg m <sup>2</sup> ]	Tower moment of inertia
$J$	[kg m <sup>2</sup> /s]	Tower angular moment of inertia
$M$	[kg]	Total mass
$b$	[m]	Distance between motor centre of mass and tower centre of rotation
$c_v$	[kg/s]	Axial Force on the blade linearized to wind
$k_v$	[kg m <sup>2</sup> /s]	External torque over blades linearized to wind
$c_\omega$	[kg m/s]	Axial Force over blades linearized to motor rotor speed
$k_\omega$	[kg m <sup>2</sup> /s]	External torque over blades linearized to motor rotor speed
$c_t$	[kg m/s <sup>2</sup> ]	Axial force over blades linearized to blade pitch
$k_t$	[kg m <sup>2</sup> /s <sup>2</sup> ]	External torque over blades linearized to blade pitch
$c_r$	[kg m/s]	Water radiation dumping referred to pitch rate
$c_{rs}$	[kg/s]	Water radiation dumping referred to surge rate
$k_{mooring}$	[kg/s <sup>2</sup> ]	Mooring stiffness
$k$	[kg m/s <sup>2</sup> ]	Platform hydrostatic stiffness

Tab. 5 List of linearized equations' terms

Three additional assumptions have been made:

- $F_0$  (the force generate by wind over wind turbine blades) is neglectable
- The control torque can be expressed as the difference of a mean value and a variable value

$$C_{gen} = C_{gen_{mean}} - C_{gen_{var}} \quad (14)$$

- The external wind torque applied over blades ( $C_0$ ) is supposed to be equal to  $C_{gen_{mean}}$

Stating from such assumptions, the equations that will define the State Space linear model have been formulated. The external forces and torques are explicated in the following form of these equations.

$$I\ddot{\gamma} + c_r\dot{\gamma} + k\gamma = c_v b (v - \dot{\gamma}b - \dot{s}) + c_\omega b \omega + c_t b \theta \quad (15)$$

$$J\dot{\omega} = k_v(v - \dot{\gamma}b - \dot{s}) + k_\omega\omega + k_t\theta - C_{gen_{var}} \quad (16)$$

$$M\ddot{s} + c_{rs}\dot{s} + k_{mooring}s = c_v(v - d\gamma b - ds) + c_\omega\omega + c_t\theta \quad (17)$$

### 3.4 Linearized coefficients

The linearized coefficients  $c_v, c_t, c_\omega, k_v, k_t, k_\omega$  of the equations are linearized linked to different windspeeds values contained in the range  $v = [11 - 25] m/s$ . These coefficients can be easily obtained from MOST. The linearization used in this chapter concerns the windspeed  $v = 15 m/s$ . Contrarily to the previous coefficients, water radiation dumping coefficients are not likewise simple to obtain. Indeed, water radiation dumping coefficients do not depend on wind speed as the other coefficients do. MOST calculates these two radiation dumping coefficients thanks to a linear module for hydrodynamics computations. This hydrodynamic computation is performed in frequency-domain, considering the water radiation dumping coefficient as a function of pitch rate and surge rate. The mathematical function that expresses the values of the water radiation dumping referred to the pitch rate ( $c_r$ ) and to the surge rate ( $c_{rs}$ ) is shown above:

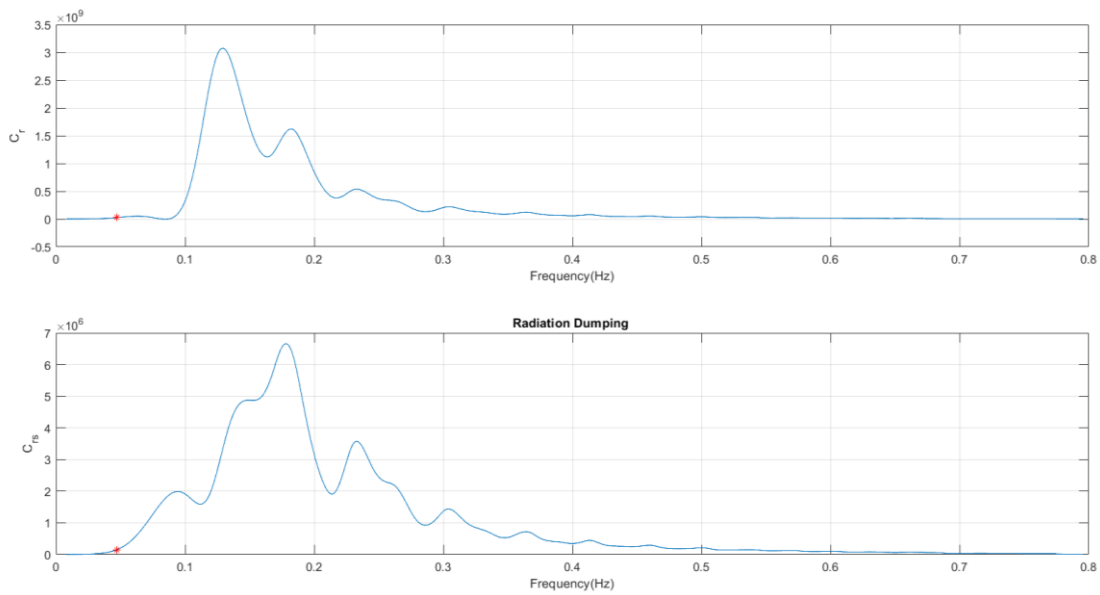


Fig. 17 Water radiation dumping coefficients as a function of frequency

These coefficients can vary according to the variation of the platform' position and velocity, likewise in relation to the waves movements. As can be seen in the graphs, the functions are non-linear. Implementing the variation of such coefficients is complex in this State Space linear model. Moreover, it has been supposed that no any significant wave is present in the simulations. Consequently, in the first instance, these two coefficients have been considered constant. The values have been obtained imposing a first try value for each coefficient in the State Space model. Then, a simulation has been ran and the time-domain response, associated with the pitch rate and the surge rate, has been transformed into a frequency-domain response through Matlab and Simulink using the function FFT (Fast Fourier Transform). In fact, this function transforms the time-domain signal in a frequency-domain signal composed of amplitude and phase. The selected value of amplitude was the peak value of pitch rate and surge rate, which represents the most critical value. Thanks to these peak amplitude values, an associated frequency for pitch rate and surge rate response can be computed. Using these frequencies, a new value of water radiation dumping has been elaborated. After four iterations, the value of water radiation dumping coefficients converged to a solution. This solution represents the coefficient associated to the most critical hydrodynamic scenario. The values obtained are expressed in the next table.

$c_r$	$c_{rs}$
$2.6885e + 07$	$1.5042e + 05$

Tab. 6 Values of water radiation dumping coefficients for pitch rate and surge rate

### 3.5 State Space model for floating offshore wind turbine

In order to rewrite the set of equation in a State Space form, it is necessary to transform the set of the three second order equations in a set of first order equations. To convert these equations is fundamental to define which variables are the states and which one are the inputs. On the one hand, pitch angle, surge displacement and rotor speed are the variables that describe the system response. On the other hand, blade pitch and control torque have been selected as inputs. The State Space form has been introduced in chapter 2 and reported below.

$$\dot{x} = Ax + Bu + Fd \quad (4)$$

$$y = Cx + Du \quad (3)$$

Chosen the important variables, the states can be defined. The chosen variables plus their first derivatives generate the states and are written according to the assumption that each state is at most the first derivative of another state. For instance, the first state is the pitch and the second is the derivative of the pitch. In this way the pitch acceleration can be expressed as the first derivative of the second state and it is a linear combination of the other states. This concept can be better understood looking at the following expression.

$$\begin{cases} x_1 = \gamma \\ x_2 = \dot{x}_1 = \dot{\gamma} \\ x_3 = \omega \\ x_4 = s \\ x_5 = \dot{x}_4 = \dot{s} \end{cases} \quad (18)$$

The inputs are then defined as follows:

$$u = \begin{Bmatrix} u_1 \\ u_2 \end{Bmatrix} = \begin{Bmatrix} \theta \\ C_{genvar} \end{Bmatrix} \quad (19)$$

The disturbance is defined by the wind:

$$d = \{d_1\} = \{v\} \quad (20)$$

To write the State Space representation can be helpful to write the three equations (15), (16) and (17) keeping the highest grade on the left side and on the other side all the other terms.

$$\ddot{\gamma} = \frac{-k\gamma - (c_r + c_v b^2)\dot{\gamma} + c_\omega b \omega - c_v b \dot{s} + c_t b \theta + c_v b v}{I} \quad (21)$$

$$\dot{\omega} = \frac{-k_v b \dot{\gamma} + k_\omega \omega - k_v \dot{s} + k_t \theta - C_{gen\_var} + k_v v}{J} \quad (22)$$

$$\ddot{s} = \frac{-c_v b \dot{\gamma} + c_\omega \omega - k_{mooring} s - (c_{rs} + c_v)\dot{s} + c_t \theta + c_v v}{M} \quad (23)$$

The State Space system is:

$$\left\{ \begin{array}{l} \dot{x}_1 = x_2 \\ \dot{x}_2 = -\frac{k}{I} x_1 - \frac{(c_r + c_v b^2)}{I} x_2 + \frac{c_\omega b}{I} x_3 - \frac{c_v b}{I} x_5 + \frac{c_t b}{I} u_1 + \frac{c_v b}{I} d_1 \\ \dot{x}_3 = -\frac{k_v b}{J} x_2 + \frac{k_\omega}{J} x_3 - \frac{k_v}{J} x_5 + \frac{k_t}{J} u_1 - \frac{1}{J} u_2 + \frac{k_v}{J} v \\ \dot{x}_4 = x_5 \\ \dot{x}_5 = -\frac{c_v b}{M} x_2 + \frac{c_\omega}{M} x_3 - \frac{k_{mooring}}{M} x_4 - \frac{(c_{rs} + c_v)}{M} x_5 + \frac{c_t}{M} u_1 + \frac{c_v}{M} d_1 \end{array} \right. \quad (24)$$

That can also can be expressed in a matrix form as following:

$$\begin{Bmatrix} \dot{x}_1 \\ \dot{x}_2 \\ \dot{x}_3 \\ \dot{x}_4 \\ \dot{x}_5 \end{Bmatrix} = \begin{bmatrix} 0 & 1 & 0 & 0 & 0 \\ -\frac{k}{I} & -\frac{(c_r + c_v b^2)}{I} & \frac{c_\omega b}{I} & 0 & -\frac{c_v b}{I} \\ 0 & \frac{-k_v b}{J} & \frac{k_\omega}{J} & 0 & -\frac{k_v}{J} \\ 0 & 0 & 0 & 0 & 1 \\ 0 & \frac{-c_v b}{M} & \frac{c_\omega}{M} & \frac{-k_{mooring}}{M} & \frac{-(c_{rs} + c_v b)}{M} \end{bmatrix} \begin{Bmatrix} x_1 \\ x_2 \\ x_3 \\ x_4 \\ x_5 \end{Bmatrix} + \begin{bmatrix} 0 & 0 \\ \frac{c_t b}{I} & 0 \\ \frac{k_t}{J} & -\frac{1}{J} \\ 0 & 0 \\ \frac{c_t}{M} & 0 \end{bmatrix} \begin{Bmatrix} u_1 \\ u_2 \end{Bmatrix} + \begin{bmatrix} 0 \\ \frac{c_v b}{I} \\ \frac{k_v}{J} \\ 0 \\ \frac{c_v}{M} \end{bmatrix} \{d_1\} \quad (25)$$

The first 5x5 matrix is the state matrix A, the second one that is a 5x2 matrix named input matrix B and the last one is the disturbance matrix F. Since all the five states can be measured by specific sensors installed on the wind turbine, the output matrix C is an identity matrix 5x5. The feedthrough matrix D is set usually to 0 because makes the system less complex and there are many ways to observe how the input is changing during simulations. Firstly, the only input considered is the blade pitch ( $\theta$ ) and the control torque is considered constant and equal to its mean value. The modelling of the control torque ( $C_{gen}$ ) will be analysed in the next chapter. If the second input is neglected, it is necessary to consider only the first column of the matrix B. Hence, in this chapter the matrix B and the input vector u are considered as follows:

$$B = \begin{bmatrix} 0 \\ \frac{c_t b}{I} \\ \frac{k_t}{J} \\ 0 \\ \frac{c_t}{M} \end{bmatrix} \quad u = \{\theta\} \quad (26)$$

### 3.6 State Space model simulation

The State Space model can be represented in Simulink with a default block named “state space” or following the scheme presented in Fig. 12 of the paragraph 2.8 of the chapter 2. In this case, the second option has been chosen. The State Space Simulink scheme can be seen in Fig. 18.

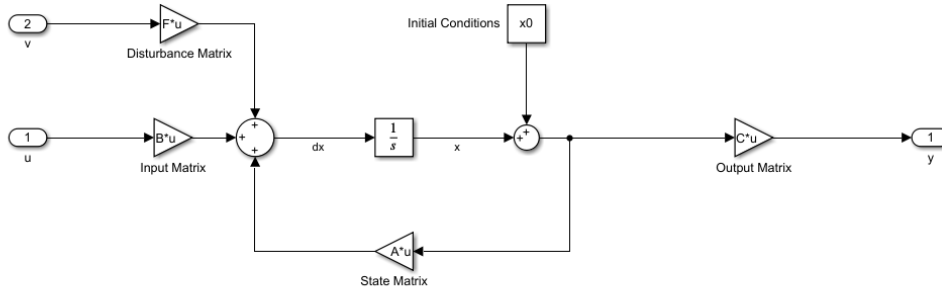


Fig. 18 Simulink scheme of the FOWT State Space model

Where  $v$  is the disturbance represented by the wind speed,  $u$  is the input represented by the blade pitch,  $x_0$  is the initial condition of the state vector and  $y$  is the output vector which contains the result of how the states vary during the simulation.

This model is based on steady state equations. For this reason, once defined the initial conditions  $x_0$ , the inputs  $u$  and the disturbance  $d$ , the model will try to let the states return to the steady state ( $x = [0]$ ). In fact, if the state vector is equal to 0, this means that there are no perturbations in relation to the value that states should have in steady state conditions. For instance, in order to test the model an input equal to 0 has been imposed, resulting in the fact that there are no variation compared to the steady state value of the blade pitch. However, a little perturbation can be imposed to the states, with the purpose of analysing how the system responds to them. For this reason the initial conditions  $x_0 = [0.1 \ 0.1 \ 1 \ 0.1 \ 0]$  is set to simulate perturbations of the initial value of the states. Moreover, the disturbance related to the windspeed has been imposed to be a step function of value 1 for 20 seconds. Consequently, a variation to the steady state value of the wind  $v_0 = 15 \frac{m}{s}$  of  $1 \frac{m}{s}$  for 20 seconds has been added. The pitch and pitch rate results have been converted from  $[rad]$  to  $[deg]$  and from  $[\frac{rad}{s}]$  to  $[\frac{deg}{s}]$  respectively. The simulation time has been set to 1000 s with a time-step of 0.5 s. The result is shown in the following figure.

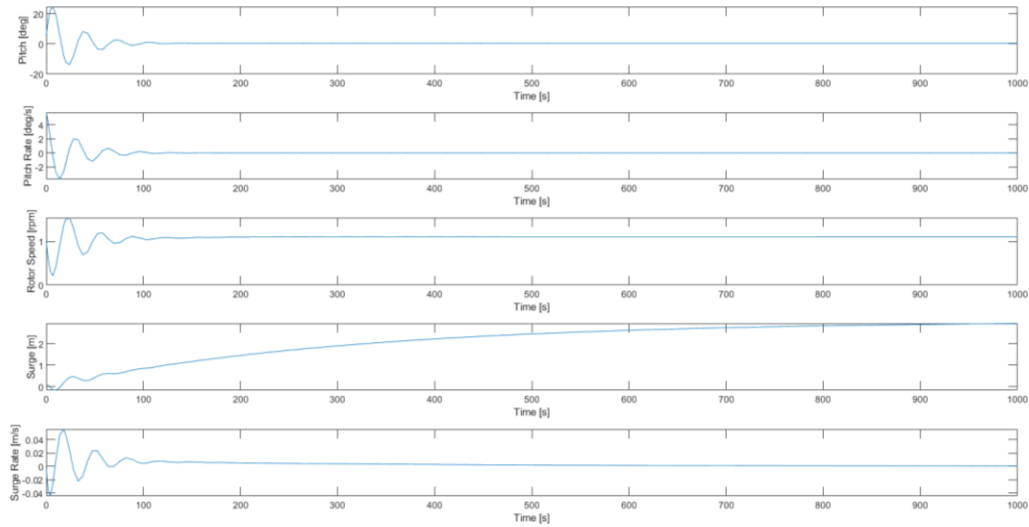


Fig. 19 Results of the open-loop State Space model

As can be seen not all the states of the open loop system return to their steady state value. In fact, the rotor speed fluctuates around the initial value of 1 rpm, but then the value remains 1 rpm. This means that it does not return to the steady state value ( $\omega = x_3 = 0$ ). The same can be observed about the surge value, which converges to 2 m. These results suggest that the system is stable but needs a controller or a regulator to return to the steady state once the disturbance is over.

### 3.7 LQR for floating offshore wind turbine

In order to stabilize and control this open loop system, a Linear Quadratic Regulator (LQR) has been developed. As discussed in the previous chapter, this feedback controller regulates and stabilizes the system varying the input as a function of the value of the states through a gain at each time step.

In this case, the State Space model does not need to be stabilized because the real part of all the eigenvalues of the state matrix (A) results to be negative.

To be designed, the LQR requires that the system has two characteristics namely controllability and observability. For what concerns such aspects, it is necessary to understand if the system A is controllable through the input matrix B and if it is observable through the output matrix C. The system is controllable if the rank of the controllability matrix ( $Co$ ) is equal to the rank of the State matrix A and it is observable if the rank of the observability matrix ( $Ob$ ) is equal to the rank of A matrix. If the system is not controllable a LQR cannot be developed. Though, if the system is

not observable it is possible to develop a LQR control but it needs to be associated with an observer in order to function. Two built-in functions exist in Matlab to calculate the  $Ob$  and  $Co$  matrices and are respectively “*obsv*” and “*ctrb*”.

For this system, the rank of the controllability and observability matrices are both equal to the rank of the state matrix and the system is observable and controllable. The LQR can be designed without the need for an observer and this is possible because all the states are measurable. However, it is not always possible to measure all the states because, to do so, too many sensors are required.

In order to develop a LQR gain it is necessary to design the Q and R matrices introduced in the chapter 2. The Q matrix is the weight matrix associated with the states, the R matrix is associated with the inputs. Since the aim of this controller is to maximize and stabilize the power production of the wind turbine in MOST, the first step was to give importance to the optimization of the states that could affect this effect. In particular, the power production can be stabilized if the rotor speed fluctuations are reduced likewise if the pitch rate tends to stabilize very quickly. For this reason, the first try values for the weights of Q gave more importance to the states  $x_2$  (pitch rate) and  $x_3$  (rotor speed) and less importance to the others. Since Q is a diagonal matrix, only the values along the diagonal have been reported in the Tab. 7. Concerning the input, the value has been set on 1 which is the most common first try value for this type of design.

$Q_{11}$	$Q_{22}$	$Q_{33}$	$Q_{44}$	$Q_{55}$	$R$
0.1	100	100	0.1	0.1	1

Tab. 7 First try values for Q and R matrices

With these values the gain can be computed, thanks to the Matlab built-in function “*lqr*”. This function takes A, B, Q, R as inputs and calculates the gain LQR matrix K. Then, the LQR gain obtained in this way can be implemented as a feedback controller in the Simulink open-loop model. This model with a feedback control is a closed-loop system. Since there is only one input and five states, the gain matrix is a 1x5 matrix. The values of this gain matrix are reported in the following table:

$K_{11}$	$K_{12}$	$K_{13}$	$K_{14}$	$K_{15}$
-16.7122	9.8253	-9.2697	-0.0198	-0.3294

Tab. 8 Values of gain matrix K linearized around 15 m/s

Each value of the gain matrix  $K$  is multiplied for the corresponding state, then all the values are summed in order to obtain the new input for each time unit.

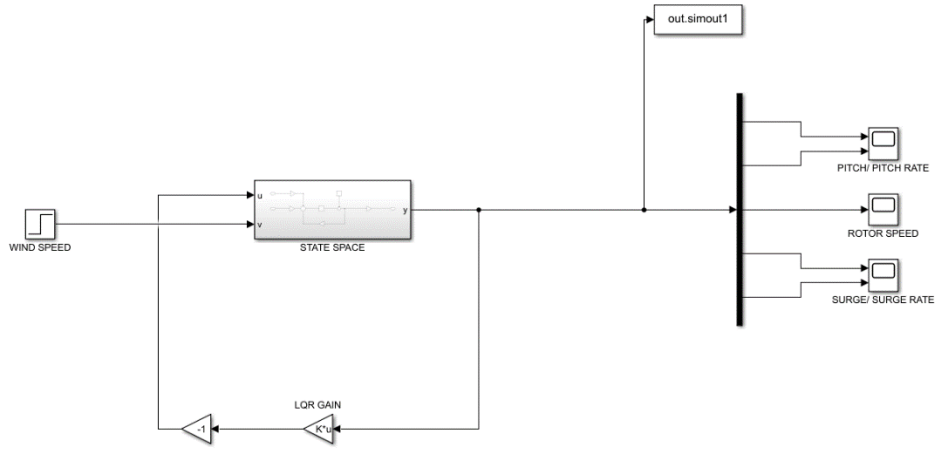


Fig. 20 Closed- loop State Space system with LQR feedback controller

The results given from this system with the same disturbance and initial conditions are showed below.

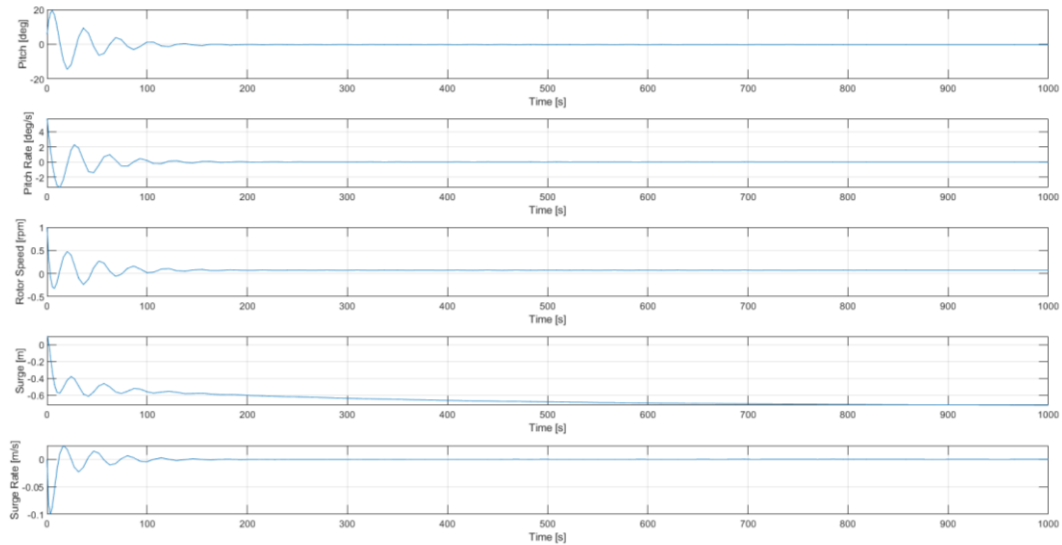


Fig. 21 State Space closed-loop simulation

It is observable that given these values also the surge variations are notably reduced compared to the results obtained in the open-loop simulation. Thanks to this controller the rotor speed tends to a near-zero value while in the open-loop simulation the rotor speed tends to a value of 1 rpm. As result, thanks to the LQR, the system after some perturbations returns to its steady state value.

Nonetheless, analysing the rotor speed response, it is visible that the reached value is not zero, as can be seen in the following graph.

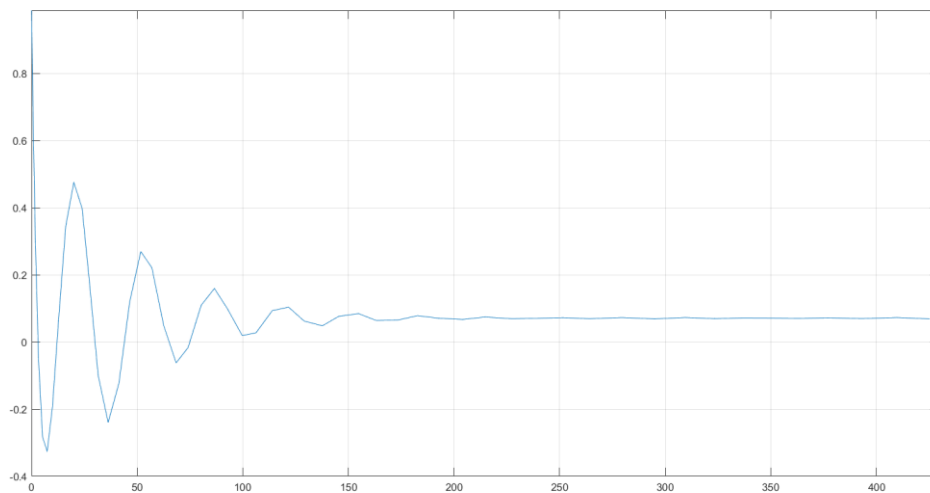


Fig. 22 Rotor speed closed-loop simulation response

If the LQR is implemented in the MOST model a relevant problem can arise. Such a issue will be discussed in the next section. In order to delete this error an LQR with integral action was designed. This controller will be analysed in the next chapter.

### 3.8 Implementation of LQR in MOST

Given the LQR gain designed, it was necessary to implement it in MOST in order to generate its new controller. This controller takes as input the values of pitch, pitch rate, generator rotor speed, surge and surge rate and multiplies it for the gain matrix  $K$ . This regulates the blade pitch input for the Voltorn US 15 MW at each time step during the simulation. The scheme of the MOST LQR controller is presented below.

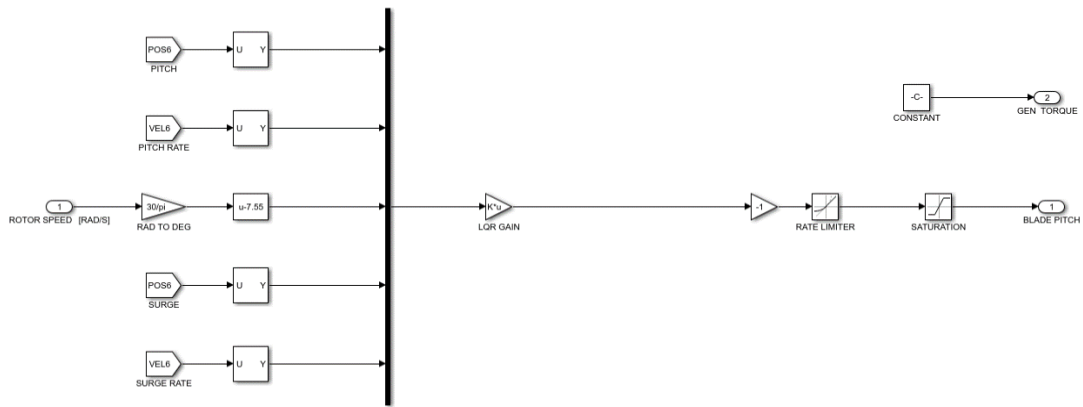


Fig. 23 Scheme of LQR controller implemented in MOST.

As can be seen the module takes the positions and velocity of the platform from another module. The rotor speed is also an input of this controller but it requires a conversion because in MOST its unit of measurement is [rad/s] while in the linearized model was [rpm]. A bias block has been included in the rotor speed line. This block helps the controller to follow the nominal rotor speed which is  $\omega_{nom} = 7.5574 \text{ rpm}$  for the Volturn US 15MW. A rate limiter and a saturation have been introduced in order to avoid extreme excursions of the blade pitch angle. The selected value are:

Saturation		Rate limiter	
Upper limit [deg]	Lower limit [deg]	Rising slew rate [deg/s]	Falling slew rate [deg/s]
90	0	7	-7

Tab. 9 Parameters for Saturation and Rate limiter blocks

The control torque is supposed to be constant. The value of this torque is calculated from MOST in the aero-loads module, which produces a series of values for some sampling values of the rotor speed. These values are showed above:

Control Torque [MNm]	Rotor Speed [rpm]
0	0
0	4.5000
8.5279	5.0328
11.1789	5.7342
14.1640	6.4447
17.4999	7.1559
19.3463	7.4951
19.6240	7.5574
19.6240	9.0000

Tab. 10 Values of Control Torque as function of generator rotor speed

The following graph shows the trend of the Control torque.

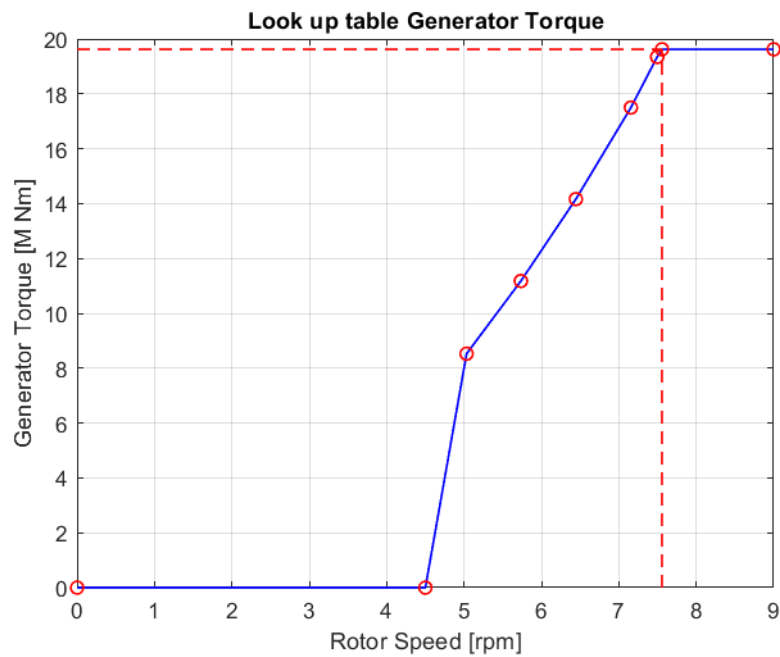


Fig. 24 Control Torque as function of generator rotor speed

The results of the simulation are expressed in the following figure.

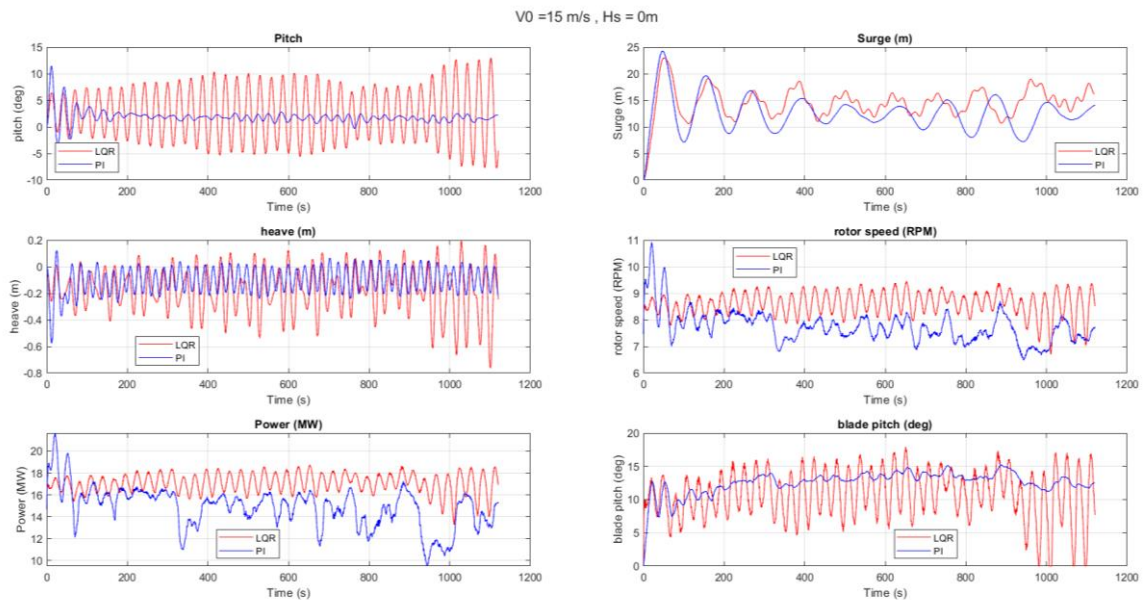


Fig. 25 Comparison MOST results with PI controller versus MOST with LQR controller

In the plots above it can be noticed that LQR controller guarantees the obstinance of a more constant generated power compared to the one obtained with the PI controller. Though, the platform pitch and heave are more oscillating if this LQR controller is applied to the model. Furthermore, also the blade pitch angle is much more irregular than the one obtained with a PI control. Concerning the power production, it can be underlined that the values obtained with the LQR controller are more stable than the ones obtained with a PI controller. However, these values fluctuate around 17 MW, which is a too high value for the Voltun US 15 MW. This effect can be explained looking at the rotor speed results.

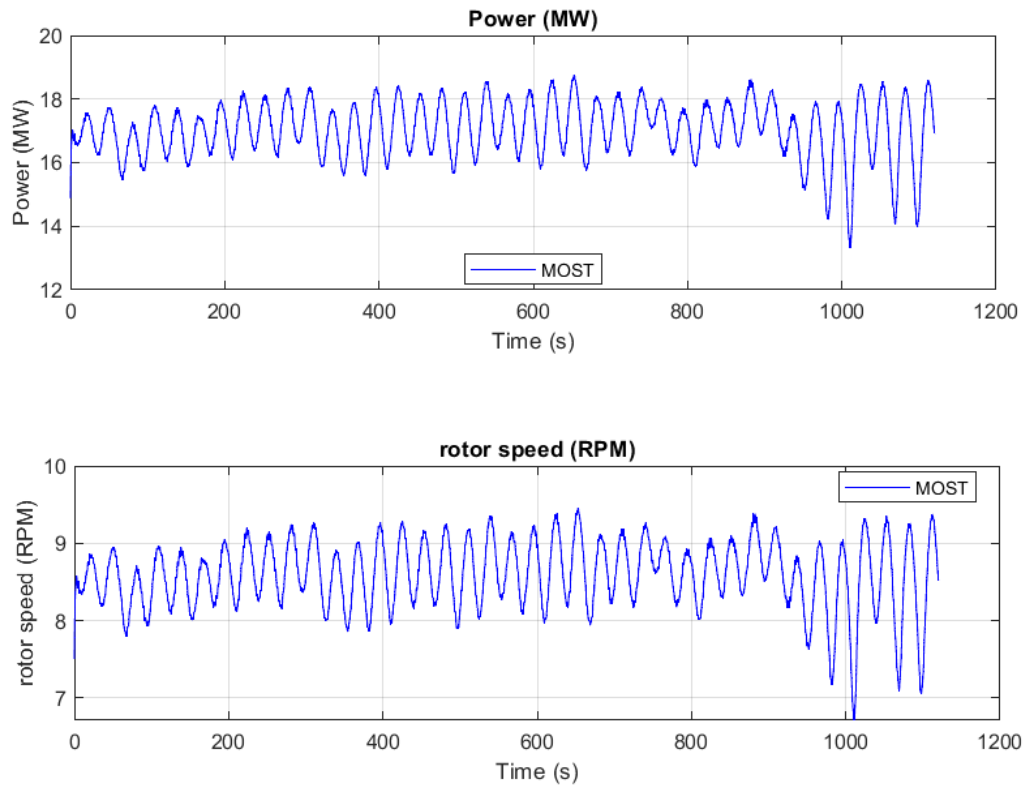


Fig. 26 Rotor Speed and Power production results of FOWT with LQR controller

As clearly emerges the controller does not follow the rotor speed value ( $\omega_{nom} = 7.55 \text{ rpm}$ ) that was set. Indeed, this value oscillates in the range of approximately [8-9] rpm; sometimes reaching lower values. Due to the fact that the rotor speed is directly related to the power, the increase of this value increases as well power production. Such a phenomenon occurs because the lack of the integral error of the rotor speed determines the incapacity of the bias block to catch the nominal value. One of the simplest ways to deal with this issue is to add an integral action to the LQR control. Consequently, a Linear Quadratic Regulator with Integral action (LQRI) has been developed and will be in depth discussed in the next chapter.

# Chapter IV

## LQR controller and linear model optimization

In this chapter different optimizations of the model will be explored and presented. Firstly, the LQRI controller will be presented and implemented. Secondly, results about linearization with different wind speeds and a gain scheduling controller will be analysed. Additionally, the results addition of the control torque input will be discussed.

### 4.1 LQR with Integral action design

The aim of the LQRI is to track rotor speed errors and to better chase the desired nominal rotor speed value. Thanks to this correction also the power production should reach the desired values. The LQRI adds to new states to the original ones, which represent the integral value of the selected states, marking the difference with the LQR. Hence, the LQRI regulates the input as a function of both the original states and the new states. This notion is better explained in the following figure.

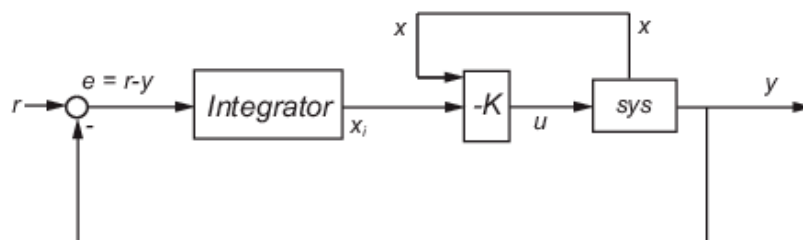


Fig. 26 Scheme of a generic LQRI [20]

The figure also shows a reference signal ( $r$ ) which is not used for the State Space model of this work. To design the LQRI, it is necessary to add other equations to the system, in this way the integral of the desired states will be added to the original ones.

In this case only the integral of the rotor speed is required and that results in only one equation necessary to express the sixth state. Since the new state is the integral of the rotor speed, its derivative is the rotor speed which is represented by the third state  $x_3$ . Consequently, the additional equation can be written as showed in the equation (28).

$$x_6 = \int \omega \quad (27)$$

$$\dot{x}_6 = \left( \int \omega \right)' = \omega = x_3 \quad (28)$$

For this reason, it is enough to expand the A matrix by adding a row which relates the derivative of the sixth state to the third state.

$$A_i = \begin{bmatrix} A & & & & & \\ 0 & 0 & 1 & 0 & 0 & 0 \end{bmatrix} \quad (30)$$

The dimension of the new matrix is 6x6, so then the B matrix needs an additional row of 0 as its last row. The C matrix also needs an additional column of 0 at the end.

$$B_i = \begin{bmatrix} B \\ 0 \end{bmatrix} \quad C_i = [C \quad 0] \quad (30)$$

The scheme of the new system with integral action is showed below.

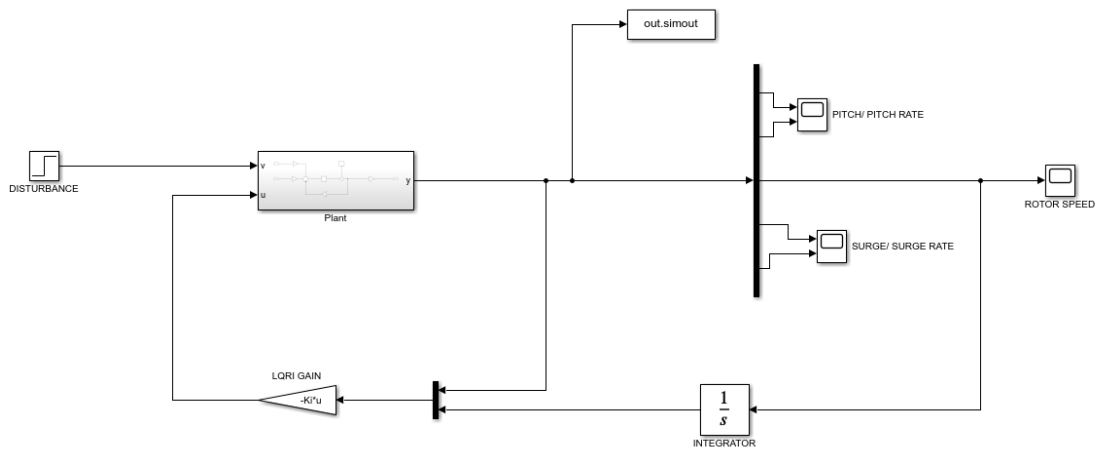


Fig. 27 Scheme of State Space with LQRI

The plant is the same of the old State Space model but the matrices  $(A_i, B_i, C_i)$  inside are the new augmented matrices introduced in this paragraph. As can be seen in Fig. 27 the sixth state is integration of the rotor speed. Similarly, the new LQRI based controller implemented in MOST will be like the one presented in the previous chapter but with an additional element which is the integral of rotor speed. This new MOST controller is showed in Fig. 28.

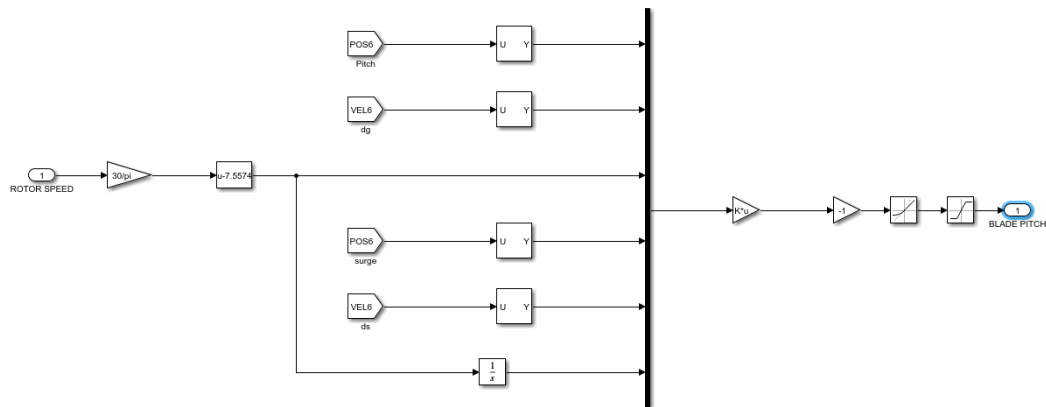


Fig. 28 Scheme of LQRI for blade pitch angle regulation implemented in MOST

## 4.2 LQRI Gain Matrix Calculation and Optimization

In this work was privileged the use of the Matlab built in function “lqr” using the augmented matrices  $A_i$  and  $B_i$  instead of the matrices  $A$  and  $B$  presented in chapter 3, given the possibility to calculate the LQRI gain matrix in different ways.

The LQRI gain matrix was developed through an optimization of the Q and R matrix parameters. It is fundamental to remind that since the states of the new augmented system are six also the new Q matrix has six elements on its diagonal.

The first step was the identification of the parameters that better influence the response of the system. Certainly, two important parameters are the ones associated with the pitch rate and the rotor speed. As shown before, the controller has a good performance if the order of magnitude of these values is  $10^2$ , and the first iteration was made through the variation of such parameters. Comparatively, the study of the parameter related to the integral of the rotor speed has been taken into account. Indeed, if the last parameter of the Q matrix is too high, the LQRI controller results to be highly unstable. As a result of it, the controller makes a relevant effort to stabilize a state which embodies only a support parameter. In fact, its function is to track only the error of the rotor speed and does not describe the physics of the system itself. For this reason, it is important to set a low value to the element of the Q matrix associated with the last state. After several iterations, it emerged that the optimal range for this value is [0.1-0.5]. Then after the analysis of all those parameters, it has been noticed that giving a good weight, to the pitch and the surge stabilization, the full system response had a positive improvement. Furthermore, assuming that the order of magnitude is  $10^2$ , the improvement of the system response has been fully reached. Conversely, in relation to the surge no any considerable oscillations resulted from the simulations. That is the reason why there is no need to stabilize the surge rate so 0.1 represents a great weight for the fifth states. For what concerns the input, the values of R matrix do not have a considerable impact on the performance of the system due to the fact they impact more on the energy cost of the input actuator. The energy expense necessary to vary the blade pitch angle within the operative range, it is much lower than the power production, a medium-low weight for the input is a good solution. Once the order of magnitude and the optimal range of variability of the values of Q and R have been identified, several dozens of iterations have been done in order to calculate the optimal LQRI gain matrix. Within each iteration, different Q and R matrices have been used to calculate the LQRI gain to test it directly in MOST. All the following iterations were performed calibrating the Q and R values on the basis of the previous MOST results simulations, until no any improvement was observed in comparison to the previous iterations. The optimal values of Q, R and K are reported in the following tables.

$Q_{11}$	$Q_{22}$	$Q_{33}$	$Q_{44}$	$Q_{55}$	$Q_{66}$	$R$
100	100	200	100	0.1	0.5	5

Tab. 11 Optimal values of Q and R matrices for LQRI gain calculation

$K_{11}$	$K_{12}$	$K_{13}$	$K_{14}$	$K_{15}$	$K_{16}$
-16.2471	19.9967	-8.3547	-0.3949	-0.6428	-0.3162

Tab. 12 Optimal values of LQRI gain matrix linearized around 15 m/s

### 4.3 LQRI Results

Given the results of the LQRI gain matrix, the same was then implemented in the State Space model. The results of the simulation of this system were compared with the ones of the LQR feedback control model. The results are reported below.

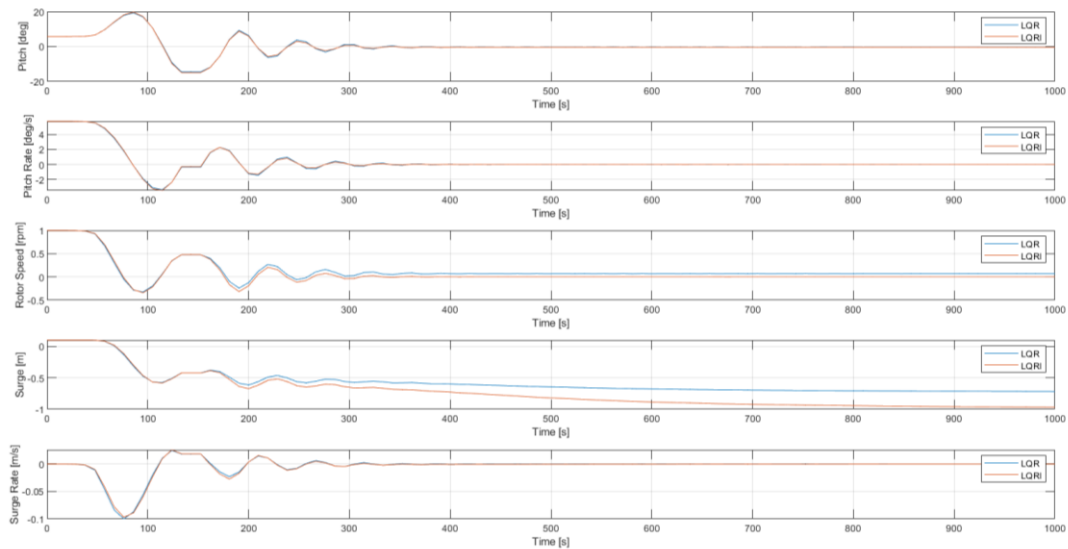


Fig. 29 Results of State Space with LQRI compared with State Space with LQR

It can be noticed that the two model responses are almost identical, except for the rotor speed and the surge response. According to the fact that the surge variation is negligible compared to the dimension of the wind turbine and that the error tracking was applied only on the rotor speed, it is interesting to take into account only the different responses of the rotor speed signal.

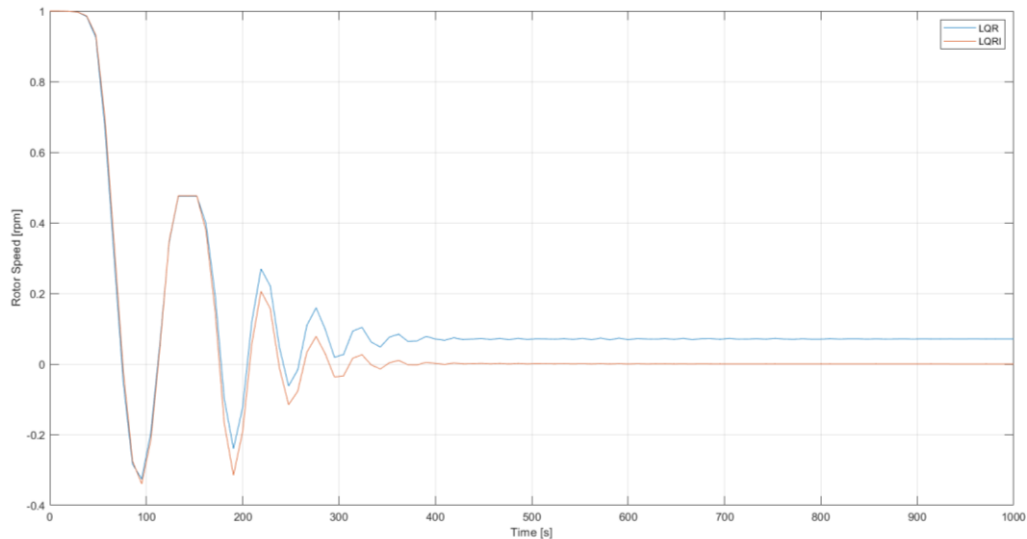


Fig. 30 Rotor speed response comparison of State Space model with LQR and LQRI

Looking at the graph above, it is clear that with the LQRI control the rotor speed value returns to the steady state value ( $\omega = 0 \text{ rpm}$ ) after 400 s. It is possible to affirm that implementing the LQRI in MOST, there is a perfect tracking of the desired nominal generator rotor speed. Furthermore, the power production oscillates around the nominal value of 15 MW and the fluctuations are considerably reduced compared to the simulations with PI controller. The results of MOST equipped with the LQRI controller are reported below.

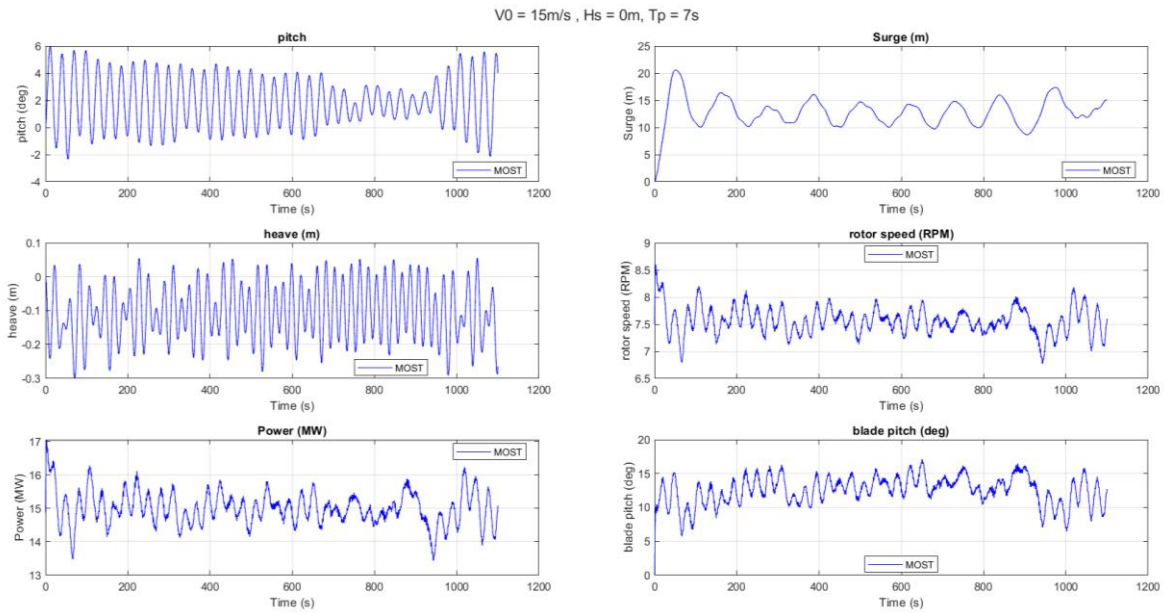


Fig. 31 MOST simulation with LQRI controller

These results show that the LQRI actually enhanced the control system of the simulator. Indeed, in the following figure a comparison with the PI results is reported to make visible this improvement. From the analysis of Fig. 32 it is clear that the LQRI based controller is effectively able to better stabilize the rotor speed of the generator around its nominal value. Consequently, this results in a stabilization of the power produced around the desired value. However, the simulator equipped with LQRI shows a more fluctuating pitch response even if slightly. The analysis about pitch gain stabilization will be discussed in the next session.

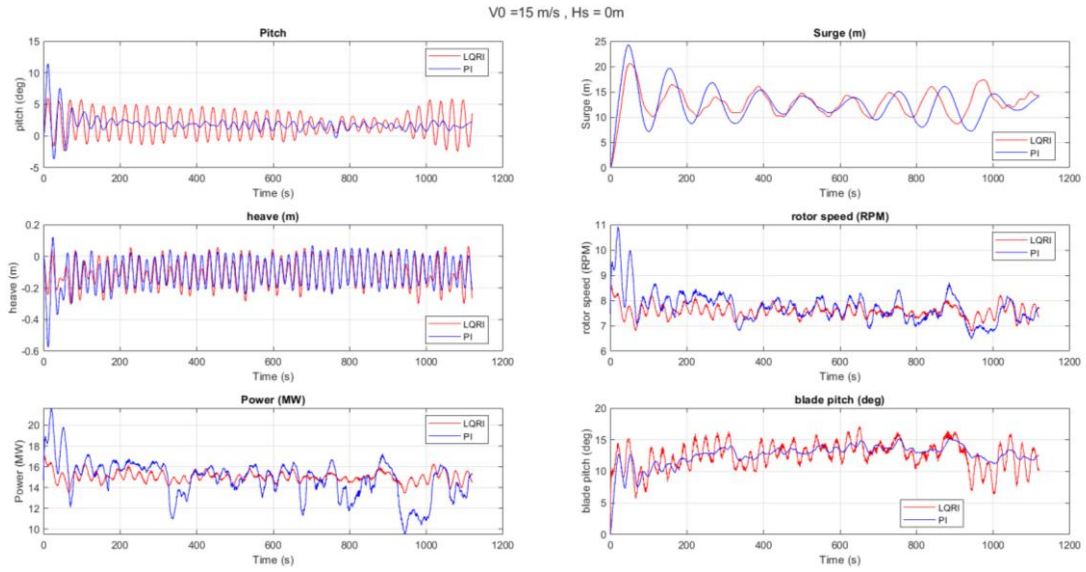


Fig. 32 Comparison between LQRI results and PI results applied in MOST

#### 4.4 Pitch stabilization with LQRI

In the previous paragraph has been identified the necessity to optimize the LQRI gain matrix concerning the platform' pitch response. Hence, a further analysis about the Q weights was required. After several trials changing the elements of the Q matrix associated with the first two states, the new weights for Pitch and Pitch Rate stabilization have been outlined.

$Q_{11}$	$Q_{22}$	$Q_{33}$	$Q_{44}$	$Q_{55}$	$Q_{66}$
8000	60000	200	100	0.1	0.5

Tab. 13 Optimal values of Q matrix for pitch stabilization with LQRI

Indeed, the new parameters of Q for pitch and pitch rate have respectively one and two order of magnitude more than the old values. Nonetheless, no variations have been made about the other parameters and the R matrix. This new set of weights generated a new improved LQRI gain matrix whose values are reported in the following table.

$K_{11}$	$K_{12}$	$K_{13}$	$K_{14}$	$K_{15}$	$K_{16}$
-45.9618	-68.5269	-9.2404	-0.3904	-0.9282	-0.3162

Tab. 14 LQRI pitch stabilized gain matrix values linearized around 15 m/s

This new LQRI gain matrix is able to stabilize both power production and platform' pitch response and this is visible in the figure below. On the account of this improvement, the LQRI based controller results to be better than the baseline PI controller in every aspect. However, this simulations has been run considering that windspeed oscillates around  $15 \frac{m}{s}$ . A gain scheduling is required to understand if the new controller works better than its counterpart considering different windspeeds.

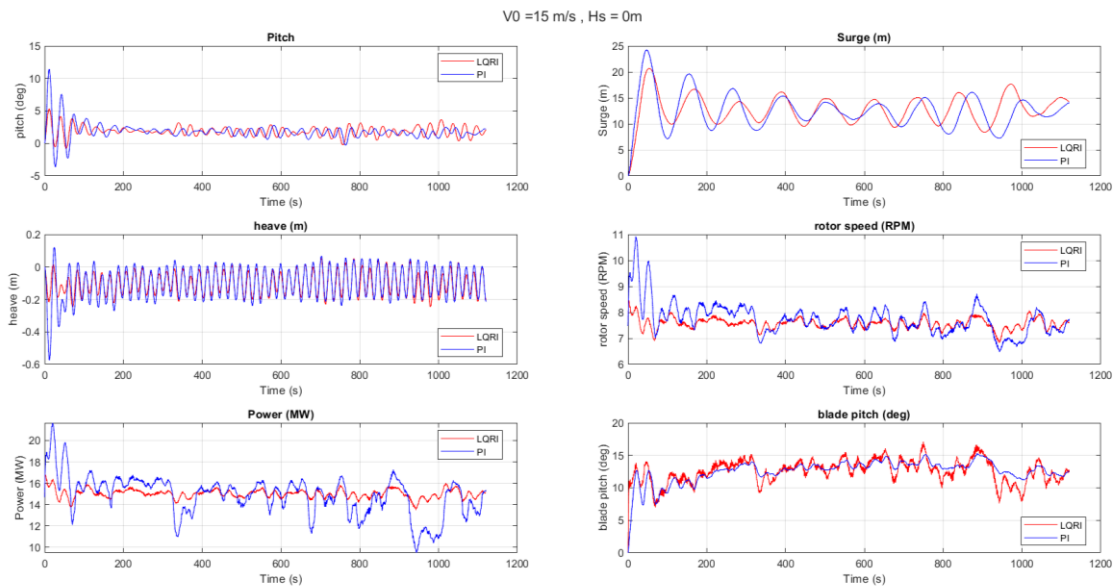


Fig. 33 Comparison between LQRI (with pitch stabilization optimization) results and PI results applied in MOST

## 4.5 Control torque control for LQRI

Up to this point, the windspeed was considered to be  $15 \frac{m}{s}$  and the control torque was a constant value not regulated by the LQRI. In this section the introduction of torque control through the LQRI will be presented.

For the introduction of a torque control in the design of the LQRI matrix was necessary to consider the State Space system as expressed in the equation (25). This system is composed of a B matrix with an additional column compared to the B matrix considered in the previous sections. Subsequently, the R matrix' weight associated to this new input was imposed to be equal to the one associated with the blade pitch. The LQRI gain matrix designed with the addition of this new input has also an additional row. Though, this row is full of near zero values because starting from such a State Space model a constant control torque is enough to regulate the system. The regulation made through the LQRI gain has to be added to the constant control torque value used in the previous version of this controller, as shown in Fig. 34.

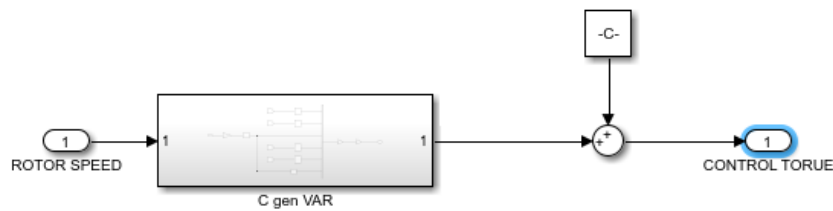


Fig. 34 Scheme of LQRI regulator for control torque

The block named “C gen VAR” showed in the figure has the same structure of the one presented in Fig. 23 for the regulation of the blade pitch angle, but it contains the LQRI gain values for the control torque. The addition of a LQRI regulation for the control torque resulted to have no significant effect on the FOWT control. Accordingly, a constant torque control is enough for this controller.

## 4.6 Gain Scheduling for LQRI

The gain scheduling is a mathematical tool which allows to store different gains, calculated for different external conditions, and to select the correct ones according to the variation of the environment. These LQRI gains have been calculated using coefficients linearized for different integer windspeed values in the range  $[11 - 21 \frac{m}{s}]$ , through which it was possible to calculate several State Space representations. Eleven gain matrices have been obtained and then repackaged. As result, a gain matrix for each state was created and generated six 11x1 matrices. Each of these new six matrices contain the gain value for a precise state at different wind speeds, as shown in the next table. The sixth state does not depend on windspeed, for this reason its matrix is filled with the same value.

Wind Speed [m/s]	Pitch ( $K_1$ )	Pitch Rate ( $K_2$ )	Rotor Speed ( $K_3$ )	Surge ( $K_4$ )	Surge Rate ( $K_5$ )	$\Omega$ Integral ( $K_6$ )
11	-52.537	-70.926	-10.735	-0.0495	0.2884	-0.3162
12	-49.306	-70.208	-10.256	-0.1308	0.0458	-0.3162
13	-47.702	-69.593	-9.8646	-0.2198	-0.2768	-0.3162
14	-46.683	-68.961	-9.5308	-0.3064	-0.6054	-0.3162
15	-45.962	-68.527	-9.2404	-0.3904	-0.9282	-0.3162
16	-45.447	-68.154	-8.9759	-0.4706	-1.2391	-0.3162
17	-45.086	-68.035	-8.7321	-0.5487	-1.5427	-0.3162
18	-44.741	-68.092	-8.4932	-0.6244	-1.8370	-0.3162
19	-44.546	-68.604	-8.2622	-0.7008	-2.1347	-0.3162
20	-44.361	69.288	-8.037	-0.7740	-2.4203	-0.3162
21	-44.235	-70.36	-7.8103	-0.8474	-2.7074	-0.3162

Tab. 15 LQRI gain values for each wind speed divided in 6 matrices for each state

The scheme of the gain scheduling LQRI for blade pitch control is shown below.

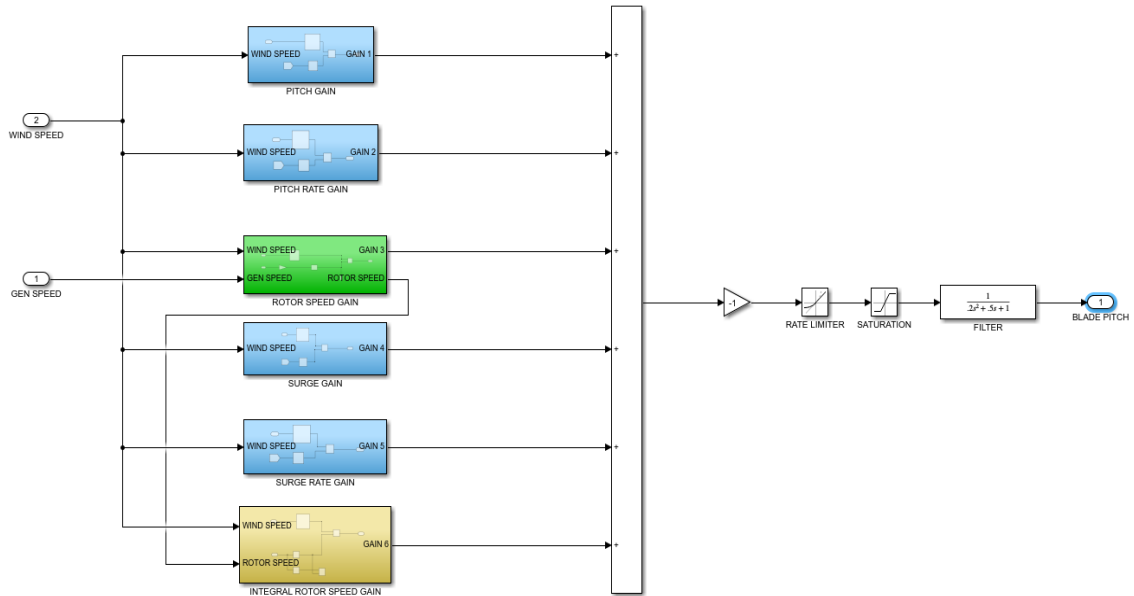


Fig. 35 Gain scheduling LQRI scheme

This controller is quite similar to the previous LQRI controller with the addition of a block for each state which selects the proper gain as a function of the wind speed. The wind speed value comes from another module which calculates it, implying the necessity to have a wind speed sensor added to the wind turbine. Since the values calculated from this module are extremely precise and fluctuating, it was necessary to apply a filter for the windspeed values in input to the controller. Moreover, another filter for the blade pitch angle output has been added. Thanks to these actions, the control signal in input to the actuator is smoother, allowing a gradual variation of the blade pitch angle over time. Concerning the gain scheduling blocks, they are all composed of a look-up table which select the correct gain as function of windspeed and multiplies it for the state, as shown in the following figure.

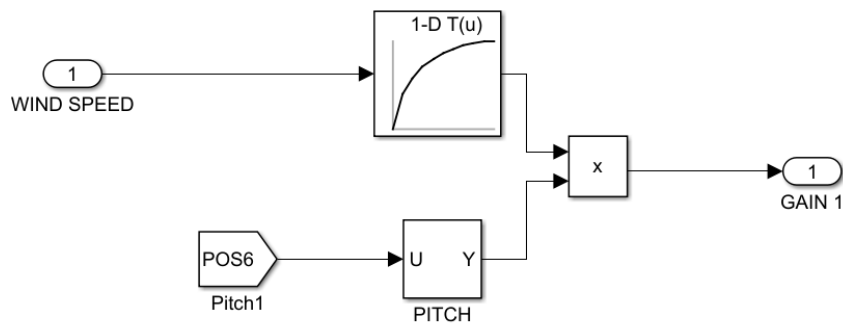


Fig. 36 Gain scheduling for pitch control

All the blocks are similar except for the rotor speed and the integral of the rotor speed blocks. Indeed, these two blocks are equipped respectively with a bias to catch the nominal rotor speed and with an integrator to better track this signal.

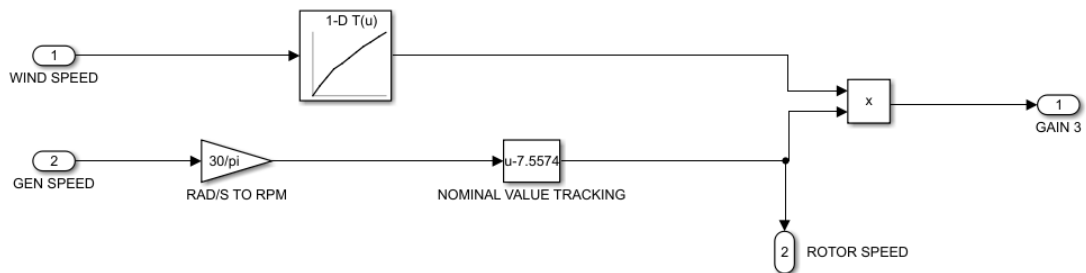


Fig. 37 Gain scheduling for rotor speed control

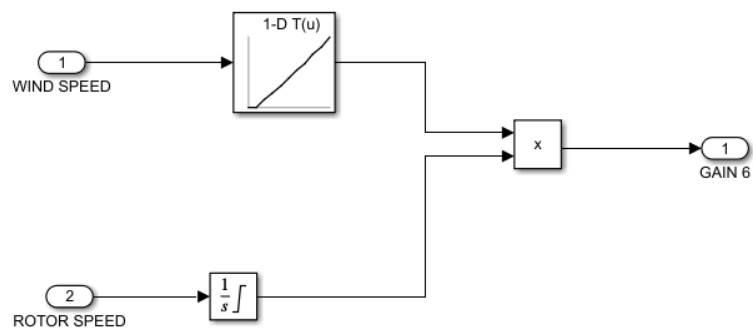


Fig. 38 Gain scheduling for rotor speed tracking

## 4.7 Gain Scheduling LQRI results

To compare this upgraded simulator with the baseline PI controller, three different wind speed ranges have been selected for the simulations. These values of windspeed oscillates respectively around:

- $V = 15 \frac{m}{s}$
- $V = 21 \frac{m}{s}$
- $V = 11 \frac{m}{s}$

The first is a medium value which has already been used for the previous simulations and does not represent a particularly critical condition. The second one represents the maximum wind speed which Voltorn US 15 MW has to face. This condition does not represent an issue for the system. On the contrary, the last range ( $V = 11 \frac{m}{s}$ ), could represent a problem for the control system. Indeed, if the wind speed reaches values below  $10.5 \frac{m}{s}$ , the blade pitch is not able to regulate the power as in the previous cases. In this condition, a control carried out only by the control torque is required. The results of these simulations are shown below.

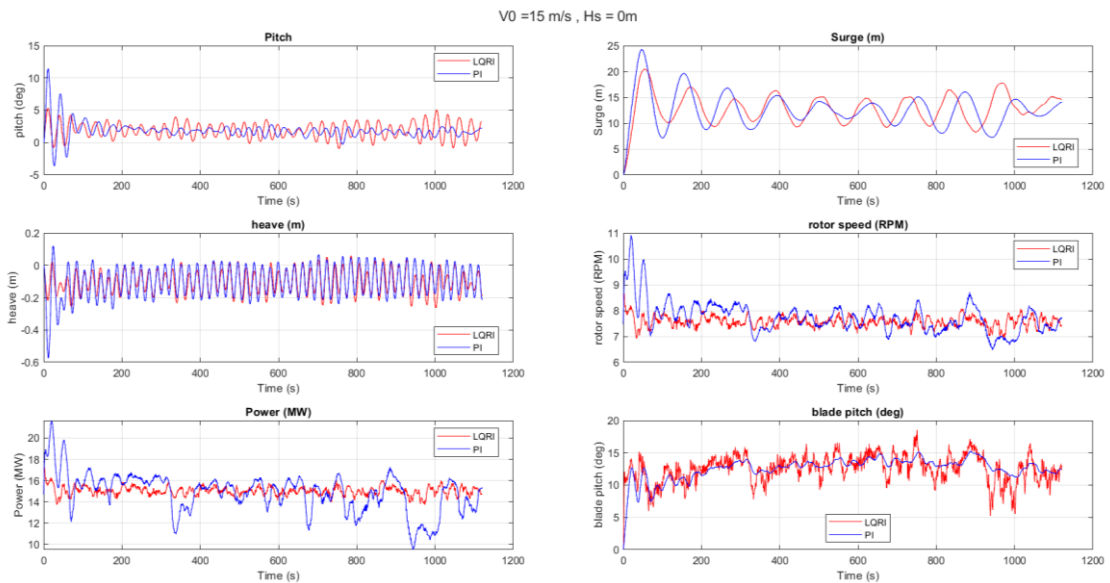


Fig. 39 Comparison PI control and gain scheduled LQRI control V=15 m/s

No any significant considerations can be deduced from this result because the wind speed is the same of the previous simulations.

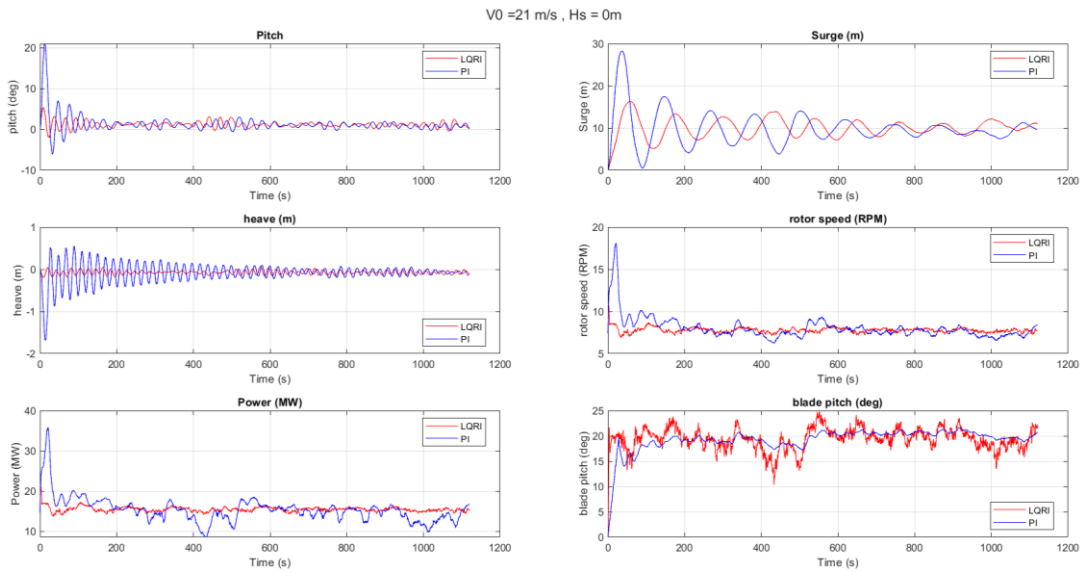


Fig. 40 Comparison PI control and gain scheduled LQRI control  $V=21$  m/s

From the Fig. 40 is visible that the blade pitch angle necessary to regulate the power around its nominal value is almost the double compared to the case in which wind speed values were around  $15 \frac{m}{s}$ .

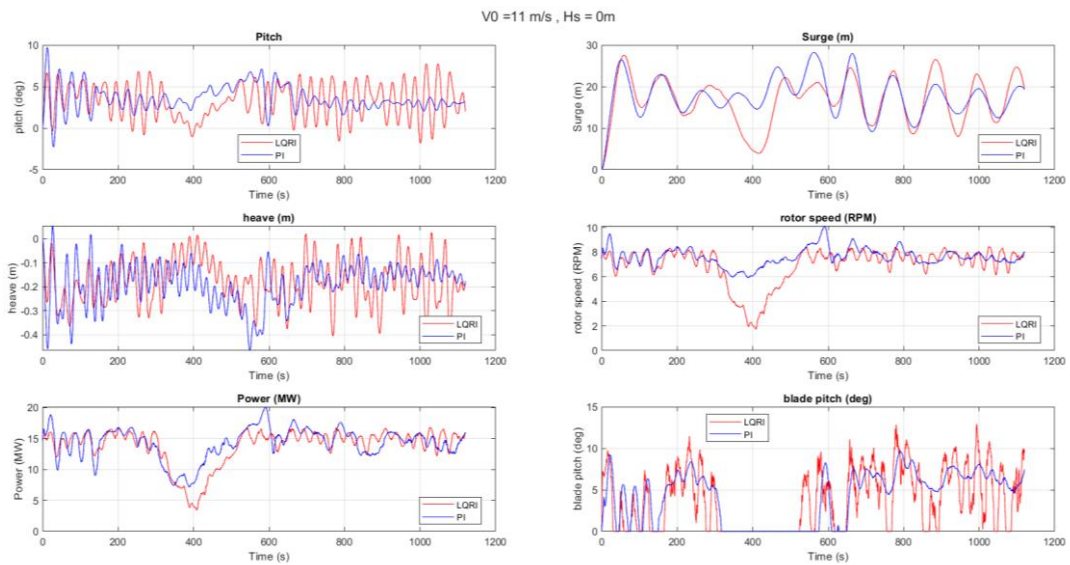


Fig. 41 Comparison PI control and gain scheduled LQRI control  $V=11$  m/s

In this last case, it is clear that none of the two controller is able to keep constant the power production around its nominal values. Indeed, in the last simulation, the wind speed assumes a wide range of values as shown in the following graph. Moreover, concerning the LQRI, it can be noticed a fall of the rotor speed value around 400 s and the same effect is also visible in the power production. That happens because around 400 s the wind speed reaches really low values. However, in such a range of wind speed values, the blade pitch controller is not able to work. To delete this negative system response, a control switch is essential.

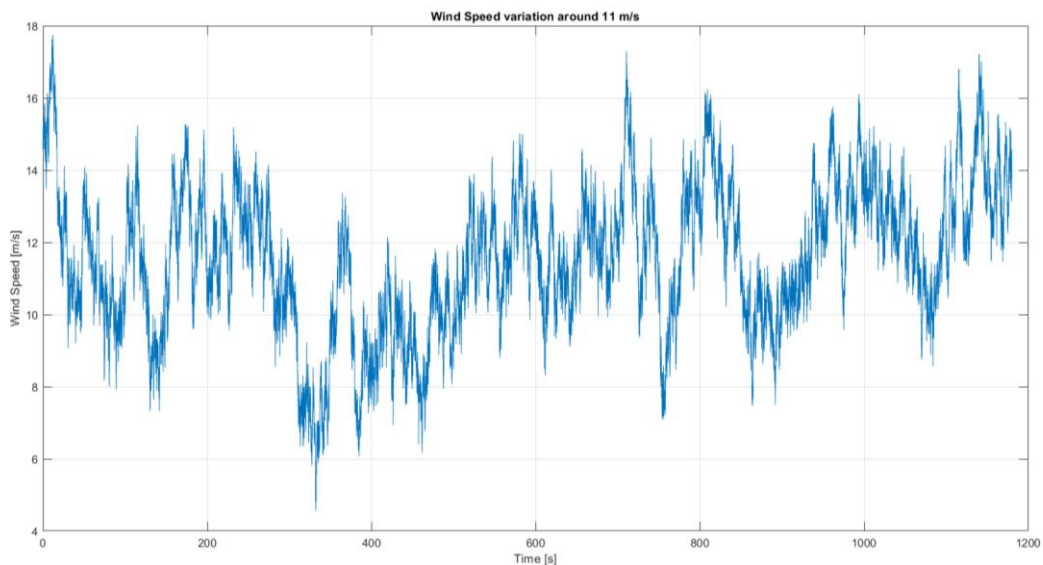


Fig. 42 Wind speed values during the simulation at  $V = 11 \text{ m/s}$

#### 4.8 Control switch

As stated before, when the wind speed reaches certain values and the blade pitch is not anymore able to regulate the power production, an exclusive torque control is fundamental. Indeed, in the following graph are reported the steady state values of this FOWT' power and blade pitch angle. From this graph it can be seen that under the wind speed of  $10.5 \frac{m}{s}$ , the power starts to decrease and the blade pitch angle fall to  $0^\circ$ .

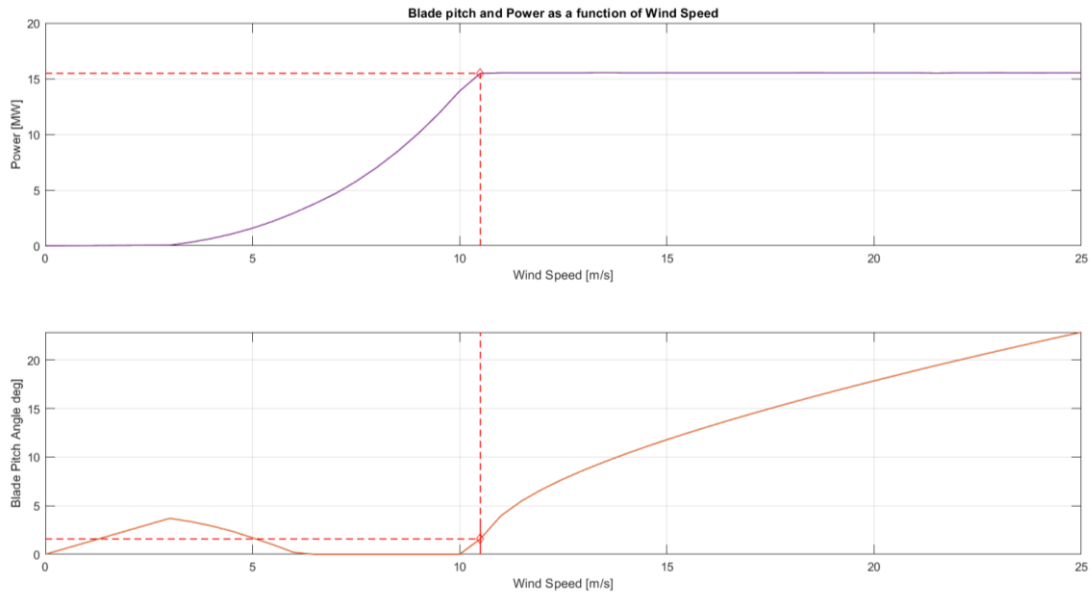


Fig. 43 Blade pitch angle and power steady state values of Voltorn US 15 MW calculated from MOST

Two different switching conditions can be used, namely:

- switching when the blade pitch angle is equal to  $0^\circ$
- switching when the windspeed is lower than  $10\text{ m/s}$

After several tests was found that the best switching condition for gain scheduling LQRI is the second one and it was implemented as showed in the following figure. A filter for windspeed was necessary to avoid sudden and useless control system output variations which could damage the actuators.

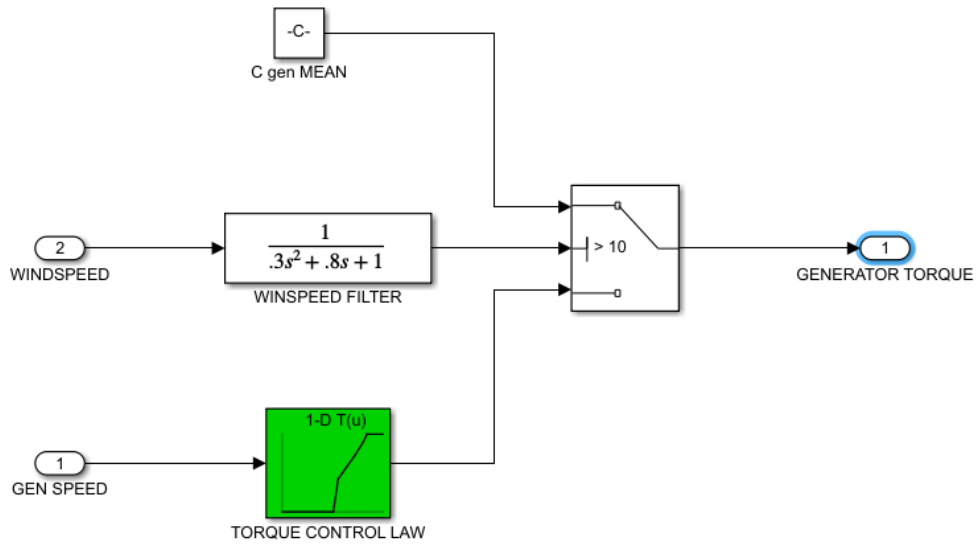


Fig. 44 Control torque control switch scheme

As can be seen in the figure above, since the wind speed has value greater than  $10 \frac{m}{s}$ , the normal control is used. On the contrary, when this condition is not fulfilled anymore, the control torque is selected from a look-up table and not constant as before. This table has on its x-axis the steady state rotor speed values and on its y-axis the required control torque values as shown in Fig. 24 in the chapter III. The complete gain scheduling LQRI controller scheme is showed in the following figure.

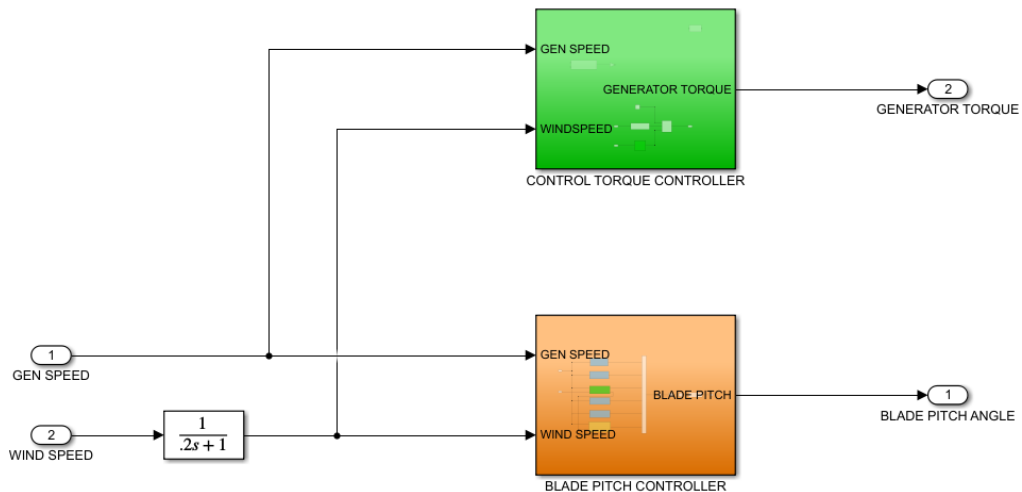


Fig. 45 Gain scheduling LQRI controller

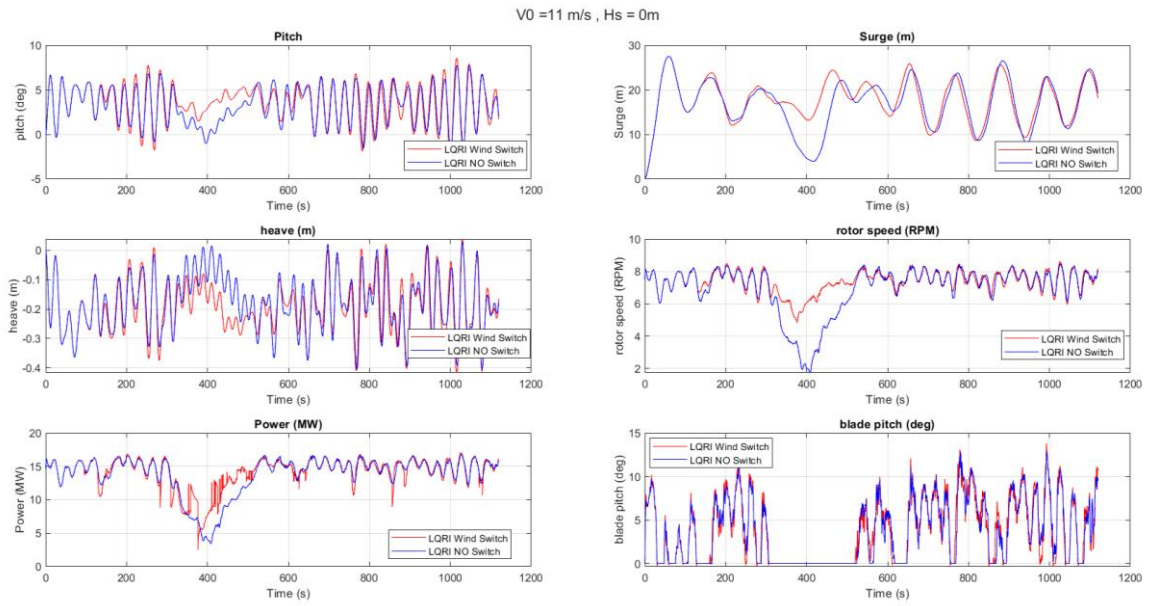


Fig. 46 LQRI with switch at  $V < 10 \frac{m}{s}$  compared with LQRI without switch.  
Simulation run for  $V = 11 \frac{m}{s}$

From the figure above can be seen that the LQRI equipped with this control switch is able to reduce the power loss. Nevertheless, this upgraded controller shows a power signal which is mightily more irregular than both the LQRI without control switch and the PI controller as shown in the following figure.

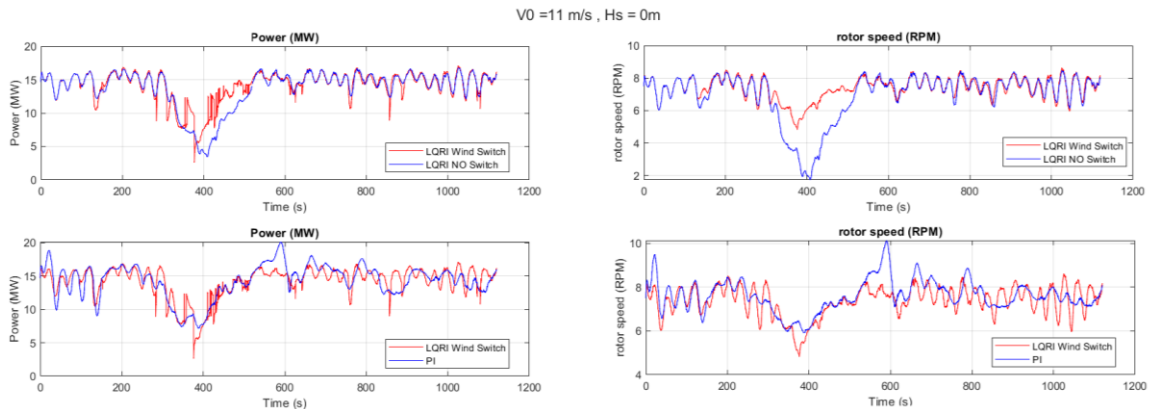


Fig. 47 Comparison gain scheduling LQRI plus control switch with PI and basic gain scheduling LQRI at  $V = 11 \frac{m}{s}$ . Differences of power production and rotor speed.

#### 4.8 LQRI with control switch without gain scheduling

Starting from the previous results, several tests of the LQRI with this control switch but without the gain scheduling module have been made. For this reason, the LQRI without gain scheduling discussed in the paragraph 4.4 was refined with a control switch and tested at different wind speeds. However, it has been noticed that in this case a blade pitch switch condition is more suitable for the control torque module.

The results of simulation with this version of the LQRI for 11 and 21  $\frac{m}{s}$  are shown below.

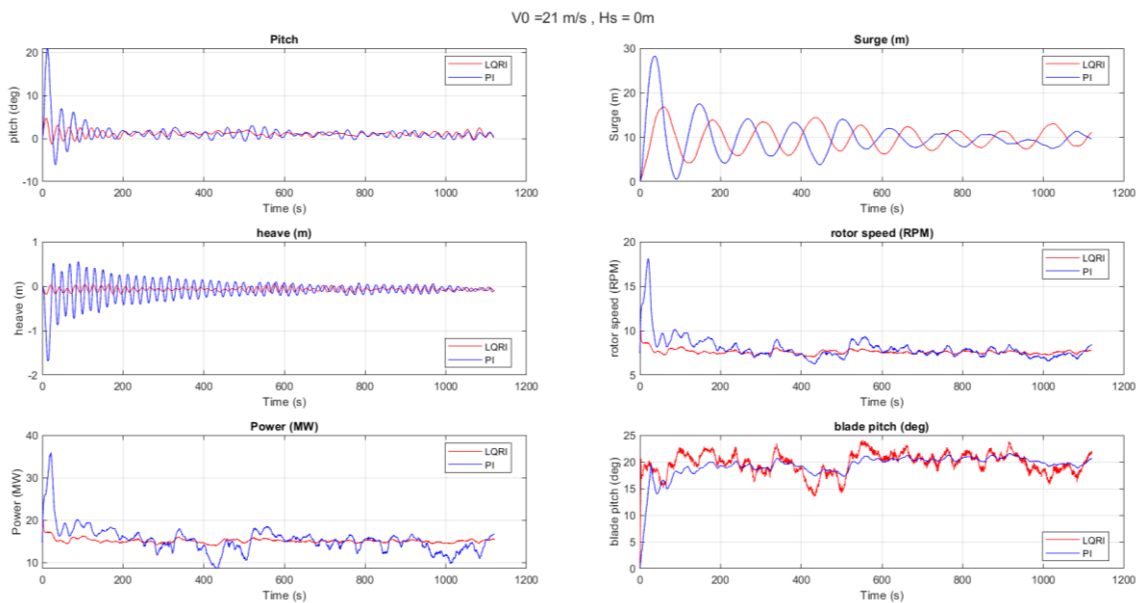


Fig. 48 Comparison LQRI plus control switch with PI at  $V = 21 \frac{m}{s}$

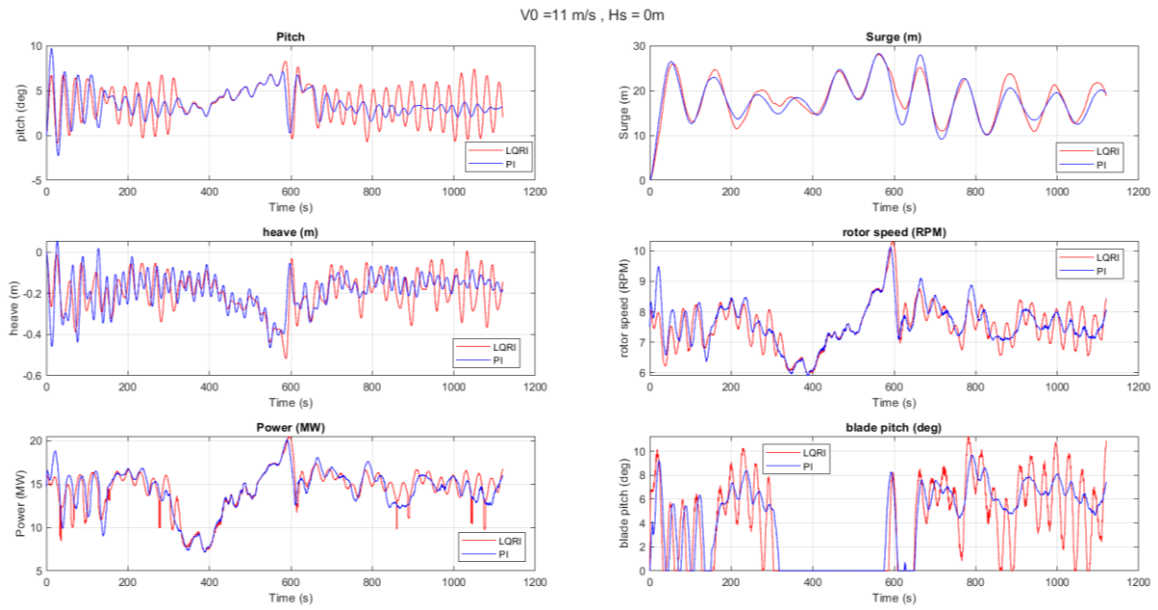


Fig. 49 Comparison LQRI plus control switch with PI at  $V = 11 \frac{m}{s}$

From the analysis of the comparison of this version of LQRI' results and the ones of the baseline PI controller at  $V = 21 \frac{m}{s}$ , it is visible that the LQRI is a better controller both for pitch and power stabilizations. On the contrary, at  $V = 11 \frac{m}{s}$ , LQRI shows a power production regulation similar to the PI but a pitch stabilization which is slightly worse than its counterpart. Despite that, the pitch oscillates in an adequate range of approximately  $[0 - 5] \text{ deg}$ . This controller has been tested with both blade pitch angle and wind speed switch conditions. Nonetheless, the second condition showed a much more irregular controller response. This event occurs due to the fact that this blade pitch controller is linearized around one value of windspeed. For this reason, it is less adaptive to variations of wind speed rather than to blade pitch angle ones.

On the basis of these observations, it can be stated that a LQRI without a gain scheduling and equipped with a control switch is a powerful alternative to the baseline PI controller. Indeed, this LQRI controller overcomes its counterpart in both pitch and power stabilization for all windspeeds superior to  $10.5 \frac{m}{s}$ . Nevertheless, when the windspeed values falls under this limit, the LQRI is still able to perform quite similarly to the PI.

The scheme of this final version of LQRI is shown below.

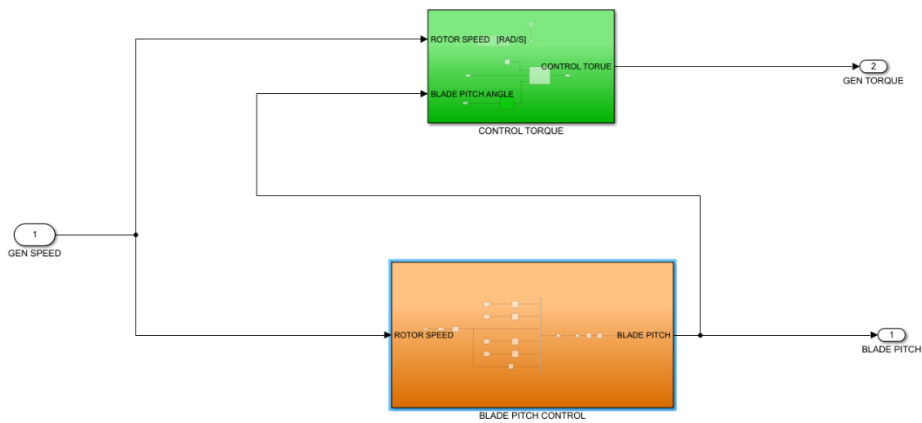


Fig. 50 Scheme of LQRI without gain scheduling for blade pitch equipped with blade pitch switch control.

In this last version of LQRI, the blade pitch control module is the one discussed in the paragraph 4.1 with the gain values shown in the paragraph 4.4. Accordingly, the control torque module has the same structure presented in the section 4.8 but with a different switch condition as displayed below.

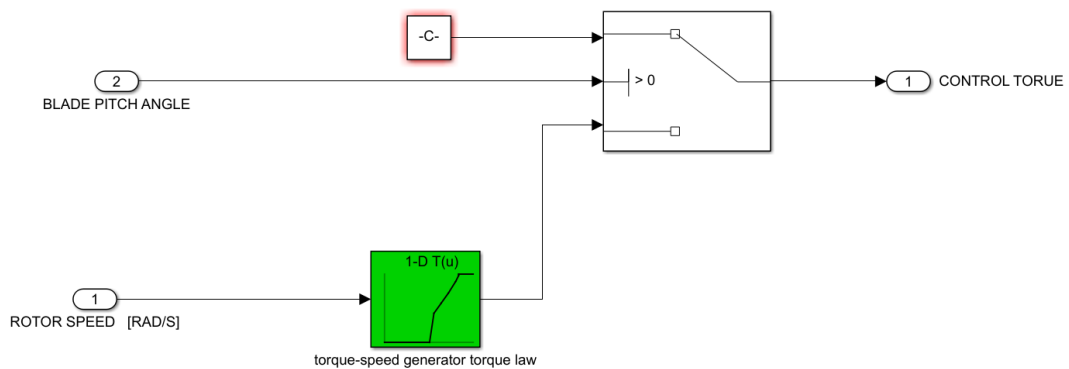


Fig. 51 Scheme of LQRI without gain scheduling' control torque module

# Chapter V

## Analysis' assumptions

In this section, the most significant assumptions discussed in chapter III will be recalled and their impact on the results will be analysed. Moreover, it will be introduced how the State Space model should change if these assumptions are deleted.

### 5.1 General analysis's assumptions

The most relevant assumptions made to write the simplified and linear State Space representation of a FOWT were:

- The wind speed is equal to  $15 \frac{m}{s}$
- The control torque is considered to be constant
- The platform' degrees of freedom considered are three instead of six
- No significant waves are considered
- The water radiation dumping coefficients are considered constant

The first assumption has already been discussed in the last sections of the previous chapter. Indeed, thanks to the gain scheduling is possible to choose the proper gain as the wind speed varies making possible to use the controller also if the wind speed is not constant. Although, in chapter IV was examined that the LQRI controller without gain scheduling works better than the one with this tool, also when taking into account the changes of wind speed. For this reason, the assumption resulted to be not influent on the controller design.

The second assumption has been likewise discussed in the previous chapter. A LQRI for the control torque regulation has been designed and presented in section 4.5. However, this regulation showed a negligible variation in control torque values and consequently this module has been deleted.

Despite that, it was also observed that when the wind speed value drops below  $10.5 \frac{m}{s}$ , the combination of constant control torque and variable blade pitch angle is not capable to stabilize the system anymore. Indeed, in that condition an exclusive control torque regulation is essential. In that regime, the control torque value changes according to the control torque law showed in the section 3.8, and this assumption had a considerable impact on the system response only in a certain range of wind speed values.

The third assumption concerns the considered degrees of freedom. In this work, the State Space model has been written considering that the platform can only have three types of movements which are respectively surge, pitch and heave. The heave has not been considered in the formulation of the State Space representation due to its negligible variations. If a 6 DoF controller is required, the design process is quite similar. Indeed, the first step is to write down additional equations which can express platform' yaw, roll and sway response. Thereafter, the negligible terms have to be deleted and the linearized coefficients, which express the relations between the old equations and the additional ones, has to be introduced. In conclusion, an accurate analysis of how the Q and R matrix weights influences the system response is required to design an optimal 6 DoF LQRI controller. Nonetheless, this design and 6 DoF will not be discussed in this work.

Concerning the assumption that no significant waves are considered, several simulations have been carried out. However, no relevant variations have been registered in the system response according to the  $H_s$  parameter modification, whose range is  $[0 - 8] m$ . For instance, in the following graph the results concerning a simulation with  $V = 15 \frac{m}{s}$  and  $H_s = 5.7 m$  and a period of the wave  $T_s = 7 s$  have been reported. Moreover, it is visible that the system response is almost the same as the one without significant waves. The last assumption requires an in depth analysis that will be made in the next section.

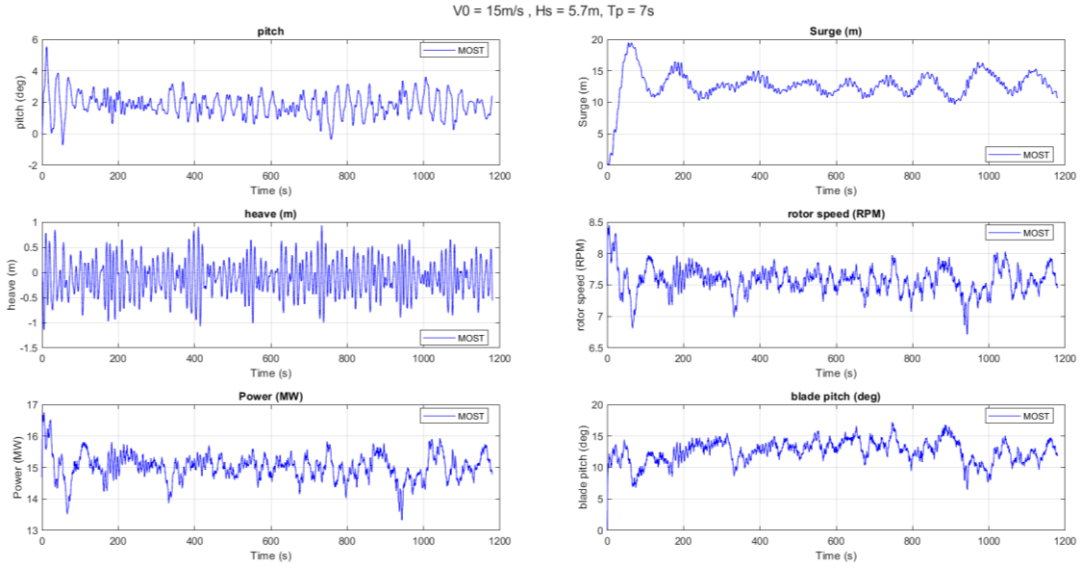


Fig. 52 MOST simulation with LQRI controller  $V = 15 \frac{m}{s}$  and  $H_s = 5.7 m$

## 5.2 State Space model with non-constant water radiation damping coefficients

The analysis about how the State Space model should change if the water radiation damping coefficients are not considered constant anymore has been conducted on a 3 DoF State Space model. However, the methodology to extend this upgrade also to a 6 DoF is analogous.

At first instance, it is important to remember that MOST is capable of calculating these radiation damping coefficients through its hydrodynamic module. Indeed, this module includes a model which computes the radiation damping forces taking as inputs the pitch rate and the surge rate. This State Space model approximates the force associated with each DoF and their combinations through 306 states. This module also generates a matrix that allows to identify which states are associated with the pitch rate, the surge rate and their combinations. In this case two states are associated with the pitch rate, four states with the surge rate and twelve with the combinations of the two velocities. Accordingly, the new State Space model for the design of LQRI has to have eighteen new *fake states* ( $\zeta$ ). These states are called *fake states* because they do not represent the physics of the system but they are just mathematical operators useful to combine radiation damping forces with the derivative of the system's DoF. In order to expand the original FOWT State Space model, three matrices are required to correlate these new states with the original six ones which are respectively:  $A_{RD}$ ,  $B_{RD}$ ,  $C_{RD}$ . The first

matrix is  $A_{RD}$ , which is a block diagonal matrix and correlates the derivative of these new eighteen fake states to the fake states themselves. Indeed, on its diagonal the first element represents the four states associated with the pitch rate, the second and the third ones represent the combination of pitch rate with surge rate and the last one is associated with the surge rate.

$$A_{RD} = \begin{bmatrix} A_s & 0 & 0 \\ 0 & A_{s\gamma} & 0 \\ 0 & 0 & A_{\gamma s} & 0 \\ 0 & 0 & 0 & A_\gamma \end{bmatrix} \quad (31)$$

The  $B_{RD}$  matrix correlates the derivative of the fake states with the original states associated with the pitch rate and the surge rate.

$$B_{RD} = \begin{bmatrix} B_s & 0 \\ 0 & B_{s\gamma} \\ B_{\gamma s} & 0 \\ 0 & B_\gamma \end{bmatrix} \quad (32)$$

The last matrix is  $C_{RD}$  which expresses the radiation damping forces, calculated by the hydrodynamic module, as linearized coefficients correlated to the fake states.

$$C_{RD} = \begin{bmatrix} C_s & C_{s\gamma} & 0 \\ 0 & 0 & C_{\gamma s} & C_\gamma \end{bmatrix} \quad (33)$$

In order to write the new State Space model it is necessary to eliminate the coefficients  $c_r$  and  $c_{rs}$  from the equations (21), (22) and (23) and to rewrite in order to have the new states in the following order:

$$x_{new} = \begin{pmatrix} \dot{s} \\ \dot{\gamma} \\ s \\ \gamma \\ \zeta \\ \omega \\ \int \omega \end{pmatrix} \quad (34)$$

This new vector contains 24 states because the dimension of  $\zeta$  is 18x1. Then after, the new state matrix  $A_{TOT}$  which represents the new State Space model necessary to design a LQRI without considering constant radiation dumping coefficients, it is expressed as following:

$$A_{TOT} = \begin{bmatrix} -\frac{c_v b}{M} & -\frac{c_v b}{M} & -\frac{k_{moor}}{M} & 0 & [C_s \ C_{s\gamma} \ \dots] & \frac{c_\omega}{M} & 0 \\ -\frac{c_v b}{I} & -\frac{c_v b^2}{I} & 0 & -\frac{k}{I} & [\dots \ C_{\gamma s} \ C_\gamma] & \frac{c_\omega b}{I} & 0 \\ 1 & 0 & 0 & 0 & \dots & 0 & 0 \\ 0 & 1 & 0 & 0 & \dots & 0 & 0 \\ B_{RD} & 0 & 0 & 0 & A_{RD} & \vdots & \vdots \\ -\frac{k_v}{J} & -\frac{k_v b}{J} & 0 & 0 & \dots & \frac{k_\omega}{J} & 0 \\ 0 & 0 & 0 & 0 & 0 & 1 & 0 \end{bmatrix} \quad (35)$$

In the  $A_{TOT}$  matrix all the dots represent rows or columns full of zeros according to the dimensions of the  $A_{RD}$ ,  $B_{RD}$ ,  $C_{RD}$  matrices. The  $B_{TOT}$  and  $C_{TOT}$  matrices, required to design the new LQRI controller, has to be expanded with columns and rows of zeros according to the dimensions of the new matrix  $A_{TOT}$ . The LQRI gain matrix can be calculated as showed in the previous chapter, however, the addition of these fake states has be intended as the integral of the rotor speed. Indeed, these states are just mathematical operators and do not represent the system response. Since the observable states are just the five states discussed in chapter III, an observer is required to use the LQRI in a State Space model. This augmented State Space model has been theorized but not designed in this work.

# Conclusions

The objective of this work was to develop a controller that could replace the MOST' baseline PI controller and that was developed from Politecnico di Torino. Indeed, MOST is a simulator for floating offshore wind turbines, developed from MOREnergy Lab for Politecnico di Torino, which has currently two different controllers both developed by National Renewable Energy Laboratory (NREL). Moreover, the aim of the design of this new controller was to overcome the PI main limitation identified as a highly fluctuating power production.

The methodology of research started by the analysis of different controllers. The LQR was selected as basic model for the design of a new controller due to its simple structure and its efficiency for FOWT applications, supported by the analysis of a robust body of literature covering such a topic. Accordingly, the FOWT physical model has been simplified through different assumptions, then linearized, and finally converted into a State Space representation. Then after, the first LQR controller was developed, implemented and tested on MOST, proving its efficiency in the stabilization of power production. However, the tests gave unsatisfactory results concerning different aspects of the functioning. For instance, the first trial showed that both power production and rotor speed exceeded their nominal values combined with a reduced pitch stabilization compared to the PI controller. These issues have been gradually solved thanks to the introduction of an integral action on the rotor speed and a repeated design of the cost function' parameters. In the first instance, a LQRI was designed to replace the LQR because, thanks to the addition of an integral action on the rotor speed, it was able to delete the error during the tracking of the desired rotor speed. Secondly, the platform pitch response was stabilized by degrees through an increasing of the weights of the Q matrix associated with pitch and pitch rate. Indeed, these weights were responsible for the platform pitch performance. After several iterations, the optimal values have been identified and the pitch was stabilized mutually to the power production.

The design of this LQRI proceeded through the reconsideration of the two assumptions that considered the wind speed and the control torque as constants. Nevertheless, both these upgrades did not prove the expected results. Indeed, the control torque showed to produce no any significant improvement to the system control. Additionally, the gain scheduling showed a degradation of the controller performance.

Another relevant issue concerned the low wind speed operative conditions. Indeed, in this regime, the blade pitch controller is not able to regulate the power production, hence a full torque control is required. In order to move from a control set to the other, it is fundamental a switch condition. Due to that, different switch conditions have been tested to solve this issue. The best condition was identified in the nil of the blade pitch angle. Consequently, the final design of this work' controller is:

- LQRI controller for blade pitch.
- Constant torque control for windspeeds greater than  $10 \frac{m}{s}$ .
- Look- up table selection control torque for windspeeds lower than  $10 \frac{m}{s}$ .
- Control switch for low windspeeds when the blade pitch angle reaches the value  $\theta = 0^\circ$ .

As a result of this work it is possible to state that the controller developed is effectively able to exceed PI controller performance for windspeeds superior to  $10.5 \frac{m}{s}$ . Nonetheless, it is also necessary to point out that it shows a similar functioning of PI when the wind speed falls under this precise value. Furthermore, an analysis of how the assumptions and simplifications of the model impacted on the controller design has been conducted.

Due to the potentiality to continue the improvement of such a model, some possible variations of the design process omitting the simplifications discussed in this work, have been formulated to create a more reliable and precise controller.

# Bibliography

[1] *A multi-objective design optimization approach for floating offshore wind turbine support structures*. **M. Karimi, M. Hall, B. Buckham and C. Crawford. 2016.** 2016.

[2] **NES FIRCROFT, “ Offshore And Onshore Wind Farms: What Are The Pros And Cons?”, 2021. [Online]. Available: <https://www.nesfircroft.com/blog/2021/09/offshore-and-onshore-wind-farms?source=google.com> . 2021.** Offshore And Onshore Wind Farms: What Are The Pros And Cons? *NES FIRCROFT*. [Online] 2021. <https://www.nesfircroft.com/blog/2021/09/offshore-and-onshore-wind-farms?source=google.com> .

[3] **2020.** Wind energy expanded 19% in 2019, with around 60 GW of new capacity. *REVE*. [Online] 2020. <https://www.evwind.es/2020/07/05/wind-energy-expanded-19-in-2019-with-around-60-gw-of-new-capacity/75563> .

[4] **2022.** Global Wind Report 2022 . *GWEC*. [Online] 2022. <https://gwec.net/global-wind-report-2022/> .

[5] **2022.** Wind energy in Europe: 2021 Statistics and the outlook for 2022-2026. *Wind EUROPE*. [Online] 2022. <https://windeurope.org/intelligence-platform/product/wind-energy-in-europe-2021-statistics-and-the-outlook-for-2022-2026/> .

[6] **2019.** Offshore Wind Outlook 2019. *IEA*. [Online] 2019. <https://www.iea.org/reports/offshore-wind-outlook-2019> .

- [7] **L. Cottura, G. Mattiazzo and G. Bracco., 2020.** *Dynamic modelling of an offshore floating wind turbine for application in the Mediterranean Sea.* 2020.
- [8] **2021.** Korea Grants First Offshore Wind Farm License”, 2021. *Maritime Insight.* [Online] 2021. <https://www.maritimekr.com/2021/08/12/korea-grants-first-offshore-wind-farm-license/?ckattempt=1> .
- [9] *A review of modelling techniques for floating offshore wind Turbines.* **A. Otter, J. Murphy, V. Pakrashi, A. Robertson and C. Desmond. 2021.** 2021.
- [10] *An efficient frequency-domain model for quick load analysis of floating offshore wind turbines.* **A. Pegalajar-Jurado, M. Borg, and H. Bredmose. 2018.** 2018.
- [11] FAST. *NREL.* [Online] <https://www.nrel.gov/wind/nwtc/fast.html>.
- [12] WAMIT Home. *WAMIT.* [Online] <https://www.wamit.com/>.
- [13] **Jonkman, J.M. 2008.** Influence of Control on the Pitch Damping of a Floating Wind Turbine. *NREL.* [Online] 2008. <https://www.nrel.gov/docs/fy08osti/42589.pdf>.
- [14] *A reference open-source controller for fixed and floating offshore wind turbines.* **N.J. Abbas, D.S. Zalkind, L. Pao and A. Wright. 2021.** 2021.
- [15] *Two LQRI based Blade Pitch Controls for Wind Turbines.* **Nam, S.Park and Y. 2012.** 2012.
- [16] State Space Representations of Linear Physical Systems. *LPSA Web Site.* [Online] <https://lpsa.swarthmore.edu/Representations/SysRepSS.html>.
- [17] **Büchi, Roland. 2010.** *State Space Control, LQR and Observer.* 2010.

[18] **Douglas, B. 2019.** State Space, Part 4: What Is LQR Optimal Control? *MathWorks*. [Online] 2019. <https://it.mathworks.com/videos/state-space-part-4-what-is-lqr-control-1551955957637.html>.

[19] *Development of MOST, a fast simulation model for optimisation of floating offshore wind turbines in Simscape Multibody.* **M. Sirigu, E. Faraggiana, A. Ghigo, G. Bracco. 2022.** 2022.

[20] **C. Allen, A. Viselli, H. Dagher, A. Goupee, E. Gaertner, N. Abbas, M. Hall and G. Barter. 2020.** *Definition of the UMaine VoltornUS-S Reference Platform Developed for the IEA Wind 15- Megawatt Offshore Reference Wind Turbine.* 2020.

[21] lqi Linear-Quadratic-Integral controller. *MathWorks*. [Online] <https://it.mathworks.com/help/control/ref/ss.lqi.html>.